doi:10.26443/seismica.v4i1.1349

SEISMICA

P-Wave Arrival-Time Tomograp[hy] Using ISC-EHB and Waveform Dat[a]

Ebru Bozdağ[1,*], Susini De Silva[2,3], Guust Nolet[4,5], Ridvan Örsvuran[1], ... Gökhan[6], Yahya M. Tarabulsi[7], Ahmed Hosny[7], Khalid Yousef[7], Abdullah Mousa[7]

[1] Department of Applied Mathematics & Statistics, Colorado School of Mines, Golden, CO, USA, [2] Department of Geophysics, Colorado School of Mines, Golden, CO, USA, [3] ... State Community College, ..., USA, [4] Université Côte d'Azur, CNRS/OCA, Antipolis, France, [5] Department of Geosciences, Princeton University, Princeton, NJ, USA, [6] Lawrence Livermore National Laboratory, Livermore, CA, USA, [7] Saudi Geological Survey, National Program for Earthquakes and Vo[lcanoes] ...

Author contributions: Conceptualization: EB, GN; Methodology: EB, SDS, GN; Data Curation: EB, SDS, ...; Resources: EB, GN, RG, YT, AH, KY, AM; Writing - Original draft: EB; Writing - Review & Editing: EB, GN, RÖ, ...; Supervision: EB; Funding acquisition: EB.

Production Editor: Carmine Galasso
Handling Editor: Suzan van der Lee
Copy & Layout Editor: Ethan Williams

Received: 3 April 2024
Accepted: 17 April 2025
Published: 23 June 2025

Abstract High-resolution seismic images are essential to gain insights ... processes and assess seismic hazards. We constructed a P-wave model, ... time), of the upper mantle beneath the Middle East and the surrounding ... tonic and geological history embodying various plate boundaries such a[s] ... zones, and strike-slip faults causing destructive earthquakes, spec... active volcanism. We use data from the ISC-EHB bulletin and onset-time[s] ... waveforms recorded in the Arabian Peninsula. The additional onset-tim[e] ... data significantly improve the resolution of the structure underneath ... the boundary between the Arabian platform and the Arabian shield down t[o] ... by slow and fast wavespeed perturbations in the upper mantle. Consiste[nt] ... the Arabian-Eurasian collision, the Red Sea rifting, the Hellenic Arc, ... lithosphere of the Red Sea and the west of the Arabian shield. Our model ... wavespeed anomalies in the lithosphere along the Red Sea to the Afar plu[me] ... mantle upwellings underneath the Arabian plate and Jordan.

1 Introduction

The Middle East and the surrounding regions, including Anatolia and the Caucasus, are formed by the amalgamation of different geological units and actively evolve through various plate boundaries and fault systems (Fig. 1). The GPS studies show ~20–30 mm/yr counterclockwise rotation of the Arabian plate and its adjoining areas of Iran, Turkey, the Aegean Sea, and the Peloponnese Peninsula with respect to the Eurasian plate, explaining the deformation related to the interaction of the African, Arabian and Eurasian plates (e.g. McClusky et al., 2000; Reilinger et al., 2006; Le Pichon and Kreemer, 2010; ... et al., 2022). The Bitlis–Zagros suture zone is one of the most remarkable tectonic features related to the closure of the Tethys Ocean. This broa[d] ... is accompanied by the subduct[ion] ... Cyprus trench system in the Med[iterranean] ... spreading at the Eastern African rift ... ocean-floor spreading at the Red Sea ... rift systems. The s... (Bozkurt, 2001; ... et al., 2010) along the Hellenic Arc ... tensional regime at Aegean and Western Anatolia.

compressional forces deriving f[rom the] Arabian plate on the East associa[ted with] the Neo-Tethys (e.g. Agard et al., 2005; Hatzfeld and Molnar, 2010) influences active dyna[mics] ... strike-slip North and East Anato[lian] ... westward escape and the counter[clockwise] movement of the Anatolian plate (Şengör et al., 1985; Reilinger et al., 2006; ... and ..., 1989 and ...; Rovida ..., 1998).

The Arabian shield borders with ... East and the Red Sea ... slow-sprea[ding] ... whose tectonic structure is sti[ll] one of the main challenges of the geop[hysics] ... Red Sea (e.g., seismic, gravity, ... sediment layer and the salt bodi[es] ... measurements and ... make the observ[ation] ... along the Hellenic transform fau[lt] ... (Augustin et al., 2021; ... et al., 2024). While some s[tudies] suggest that the Red Sea migh[t] ... Sinai ... continental rifti[ng] (e.g., Bonatti, 1985; Schettino et al., 2016; ... et al., 2012), although there is no cons[ensus] ... Western ... The geophysic... completed its rifting phase becom[ing] basin ~5–13 million years ago (Augustin et al., 2021; ...).

*Corresponding author: bozdag@mines.edu

Some models of the Red Sea suggest ... was created all the way from the ... (e.g., Augustin et al., 2021; Delaunay et al., 2024) while the spreading along the ridge ... part with limited extension ... Cochran, 1983; ... and McGuire, 1988; Almalki et al., 2015). The evolution of the Red Sea is also crucial ... volcanism in the Arabian Peninsula ... ings. Within the same context, the rifting on the Red Sea is the subject of debate. Rifting can be caused by several candidates ... the rotation of the Arabian plate ... tion underneath Zagros, or changes ... tion after subduction of the Neo-Tethys ... in the Western Mediterranean (Reilinger and McClusky, 2011). Rifting might be caused by mantle upwelling, of which the origin is also uncertain ... tion to the Afar plume with a deep origin (Montelli et al., 2004). Its connection with ... canism from a mantle plume (Chang and Van der Lee, 2011) and with collision ... canism as far north as Turkey (Şengör ...; Chang et al., 2021), using data from the Egyptian ... works, suggest the Harrats (basalt fields) may be fed from a plume-like feature.

The interaction of multiple plates driven by major boundary types (i.e., transform, subduction, convergent, collision) makes the area, extending from Anatolia and the Caucasus to Iran, one of the most seismically hazardous regions on Earth with frequent devastating earthquakes (e.g., Giardini et al., 1999; Sheldrick et al., 2000). Seismicity (e.g., Nissen et al., 2014) ... seismic hazard assessment (e.g., Giardini et al., 2018; Tavakoli and Ghafory-Ashtiany, 1999; ... Kiuchi, 2019) and regional source ... and location (e.g., Adams et al., 2009; Gök et al., 2016; Karasözen et al., 2016, 2019; Chiang et al., 2021) provide the foundation for arranging ... gating earthquake-related damage. ... acterization of seismic sources along complex ... boundaries, such as the Hellenic arc ... Zagros suture belt, has shown to be ... to large uncertainties (Engdahl et al., 2006; ... miller and Nábělek, 1996; ... miller et al., 2002) due to the uncertainties in structural models. Therefore, higher-resolution crustal ... mic models of the subduction/... within the lithosphere are crucial ... tainties in source mechanisms ... our depiction of the behavior of ... tems in the region.

The seismic activity in the study region is also complemented by active volcanism. The Harrats, located west of the Arabian plate, is the largest lava field ... area. Yet, their origin is still an ongoing debate similar to the opening of the Red Sea discussed above (e.g., ... Ball et al., 2013). The proximity of Harrats to the Red Sea and their alignment is one of the potential explanations for their origin related to the rifting process. One of the main theories on the cause ... plume, which coincides with the ... in East Africa. The volcanic ... Arabian plate and in the northwest ...

... activity explained by the channelization ... from the south to the north ... (e.g., Camp and Roobol, ... 2006; Duncan et al., 2016) ... smaller regions ... plumes ... the Arabian plate ... (Coleman ... Chang and Van der Lee, 2011) ... a sheet of mantle upwelling ... attributed to the Afar plume (e.g., McGuire, ...) ... the ... is also related to the ... by the lithosphere ... (... et al., 2019). The volcanic fields have ... (Pallister et al., 2010; Mukhopadhyay et al., 2013) ... about 21 known volcanic eruptions over 1,500 ... (Camp et al., 1987). The last eruption ... 1937 in Yemen ... 1256 AD ... Saudi Arabia (Camp et al., 1987) ... volcanic characteristic ... 2009 ... earthquake swarms ... the northwest of Saudi Arabia ... and rifting dynamics in the ... Red Sea region is ... dynamics of the ... leading to episodic magma intrusion (... Civilini et al., 2019).

One of the main ... for seismic ... earthquakes ... the 3D ... such as the ... plateau that is abundant with ... ism, and highly variable topography ... (e.g., Pasyanos et al., 2021) ... seismic wave propagation ... mic models of the lithosphere and ... are essential to understanding ... related multi- ... However, ... perspective ... complex ... basis for ... seismic ... (e.g., Bijwaard et al., 1998), surface waves (e.g., ... et al., 2014), and surface wave waveforms (e.g., ... Romanowicz, 1996; ... et al., 2003) ... The ... of ... (e.g., ... et al., 2014) ... Lei et al., 2020) ... overall ... general ... of data ... tomography ... able to address finer structures ... (e.g., Maggi and Priestley, 2005; ... et al., 2007; Simmons et al., 2012; Wei et al., 2019) the structure beneath Arabia (e.g., Al-Lazki et al., 2012), the Red Sea rifting connection ... (Chang and Van der Lee, 2011; Park et al., 2008; Kaviani et al., 2020) and the Arabian platform ... which is covered by ... (Gök et al., 2007) ... beneath the ... is challenging ... and ... Arabian ...

Figure 1 Topographic map of the study region with major tectonic un... Fault, DSF: Dead Sea Fault, H. Arc: Hellenic Arc, C. Arc: Cyprus ... (Reilinger et al., 2006). Red lines indicate ... (Bird, 2003) ... boundaries (between the A... Arabian platform and ... (Mokhtar ... 1994). The scale for GPS vectors is shown on the ...

studies in the region have taken ... models, while the P- and S-wavespeed mo...
creasing amount of seismic data ... (e.g., Bozdağ et al., 2016; ... 2010) ... Anato-
and provide higher resolution ... tomographic images inverted as pa...
ing regional body and surface waves ... (Zhu et al., 2012) and a recen...
lithospheric structure and ... Al- ... joint inversion ... tomography (e.g., ... of the M...
Damegh et al., 2004; Tkalčić et al., 2006; Hansen et al., Rodgers et al., 2014) ... or separately based
2007, 2008; Tang et al., 2016, 2018, 2019; Kim et al., 2023; ... mic P-wave tomography (e.g., Bijary ... 2011). Nev-
Kaviani et al., 2020; Pasyanos et al., 2021; Lim et al., ... ertheless, the P-wave resolutio...
2020; Celli et al., 2020). The regional models ... for the Arabian ... seismic tomography, whi...
bian Peninsula typically focus ... P-wave speed and limi...
models where surface waves can't ... S-waves ... to S-wave mod...
to improve the coverage (e.g., Chang et al., 2010; Zhang
et al., 2012) then constructed a P-wave ... In this study, we present MEP The P...
rived from their S-wavespeed mo... (Middle East P-wave ... of the Mid...
relationships between P and S waves (Chen and Pei, 2021) ... surrounding region, perform...
jointly inverted P and S wavespeed ... tomography with ... improved data c...
mography study of the African ... the ISC-EHB Bulletin (Engdahl et al., 2020) ... publishe...
Middle East, which imaged the ... by the International Seismologi...
ture of our study region. Other ... ISC) ... International Seismo...
wavespeed models of the region ... ar, 2020) ... readings of...
traveltimes (e.g., Simmons et al., 2021) and global ... waveforms of regional earthquak...
bian Peninsula. Our ISC data invo...

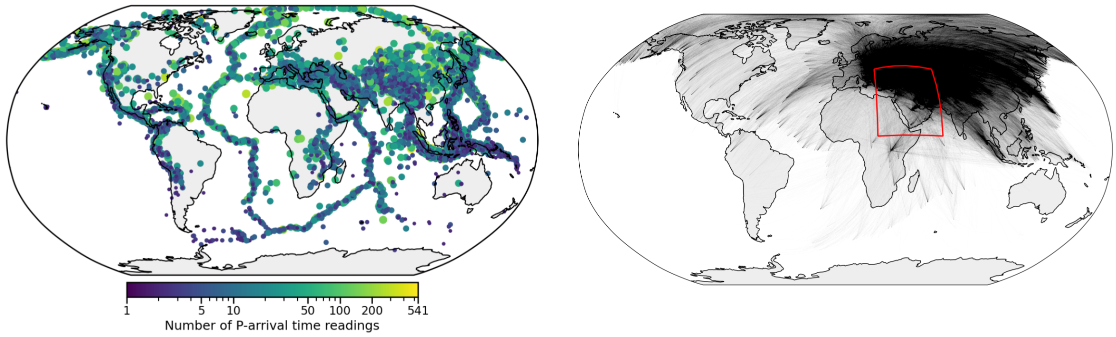

Figure 2 Distribution of the number of P-wave arrival time readings ... ing 300,513 great-circle ray paths in this study. The red box on the right m...

well-located arrival times, including regions with dense seismicity within the period 1990–2016, compared to earlier P-wave models of the region (e.g., Sandvol et al., 1998; Al-Lazki et al., 2004; Park et al., 2007; Simmons et al., 2012; Wei et al., 2019). Following studies such as Chang and Van der Lee (2011), which combine S-wave ISC arrival times with waveforms to enhance images of the upper mantle beneath the western side of the Middle East, we combine P-wave arrival times from the ISC catalog with the onset-time readings of the first arrivals from waveforms recorded by the seismic stations operated by the Saudi Geological Survey (SGS). A part of the SGS stations (the Saudi National Seismic Network, SNSN) was also used in some previous studies (Khrepy et al., 2021; Hansen et al., 2008).

The paper is structured as follows. We first give information about the data from the ISC catalog and onset-time readings from waveforms used in our inversions, followed by the tomography technique. In Section 3, we present our models constructed based on ISC data only and ISC data combined with onset-time readings from waveform data from the Arabian Peninsula. In Section 4, we discuss our observations in the context of the region's tectonics and the previous tomographic models. Finally, we summarize our results and observations in Conclusions in Section 5.

2 Data and Method

In this section, we provide some background information about our dataset, which combines P-wave arrival times from the ISC catalog with onset-time readings made on waveform data from 110 regional events recorded by seismic stations in the Arabian Peninsula, and our arrival-time tomography technique.

2.1 ISC dataset

In our inversions, we use P-wave arrival times from the ISC catalog of globally distributed earthquakes that occurred in 1990–2016. We select earthquakes with a ≥ 50 P-wave onset-time picks recorded worldwide. We ensure that no two selected events are closer than 20 km to limit cluttered ray paths ...

... onset is top 40 ... (Supplementary Material, Fig. S1) and select data ... as best as possible. In addition, ... listed in the catalog with at least ... The resulting ISC dataset consists of 16,264 ... with 300,513 P-... first arrival P-wave ... (shown in Figure 2). On the left panel of Figure 2 ... how many picks were collected at ... ISC catalog ... clearly seen ...

2.2 First-arrival P-wave onset times from waveform data

We gather waveforms of 110 regional earthquakes between 2017–2020 recorded by the seismic network operated by the SGS in the Ar... We carefully pick 2,916 onset times from the f... P waves on the vertical components ... data set. On the right panel of Figure 3, we show the distribution of P-wave arrival t... log combined with the onset-time ... forms recorded on the Arabian Pen... data processing steps applied to ... updating headers with event and ... removing the trend and the mean, ... we apply a 10 s time window around the e... theoretical arrival times of first ... on our 1D reference model AK135 (Kennett et al., 1995). We manually pick the onset times ... waves and calculate the 'P-wave d... ... information in this pro... ... of the fault, ... ISC data. ... filters are band ... 0.5 Hz–2.0 Hz ... 6-pole Butterworth f...

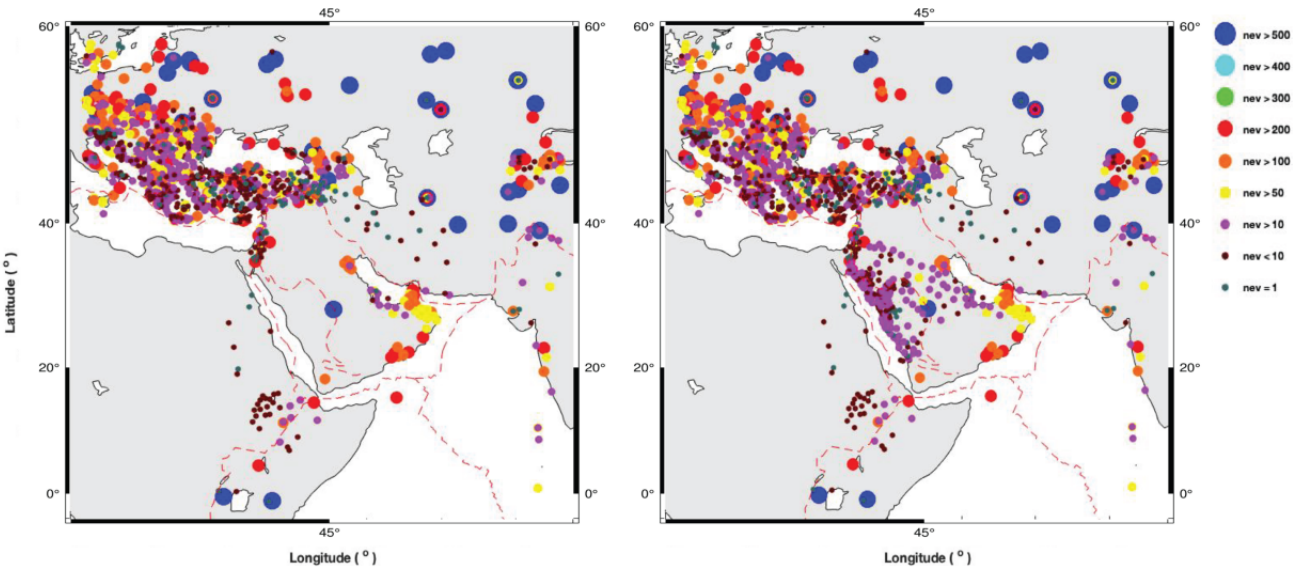

Figure 3: Left: Distribution of P-wave arrival times from the global IS[C] ... Right: Same as the left figure with the addition of the onset-time readi[ngs] ... the SGS network on the Arabian Peninsula.

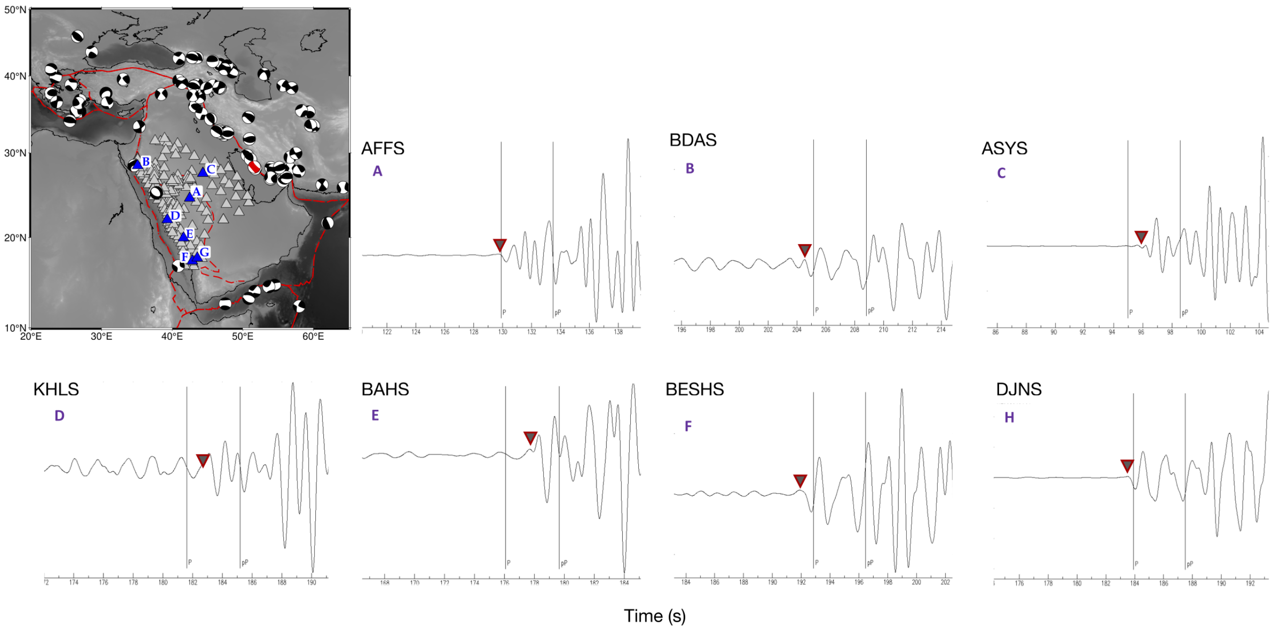

Figure 4: Vertical-component seismograms recorded at sample SGS sta[tions] for 2013 Southern Iran event ($M_w = 6.4$, depth = 12 km) shown by the red beachball. P ... recorded by the blue triangles on the map. Vertical lines ... Kennett et al. (1995) ... theoretical predictions of the first-arrival P waves. Inverte[d] ... times. Time delay input for the inversion is then defined as the ...

sharp onset times distinguishable from the ... after experimenting with various other filters (i.e., combinations of causal/zero-phase filtering at different frequency bands tested within the range of 0.2 Hz–1 Hz) including the sharp high-pass filter used by Nolet et al. (2019) tested with cutoff frequencies of 0.25 Hz–0.5 Hz. Sample vertical-component seismograms from a regional earthquake recorded by a set of seismic stations in the Arabian Peninsula ...

first-arrival P-wave onset-time ...

2.3 P-wave arrival-time tom[ography]

The depth sections of the ray dens[ity] ... including the ISC data and the onse[t] ... the waveform data in the Arabian ... sphere and mantle down to 1400 km are represent[ed] in Fig. 5. Since we assimilate onset t[imes] ... waveform data from regional eart[hquakes] ...

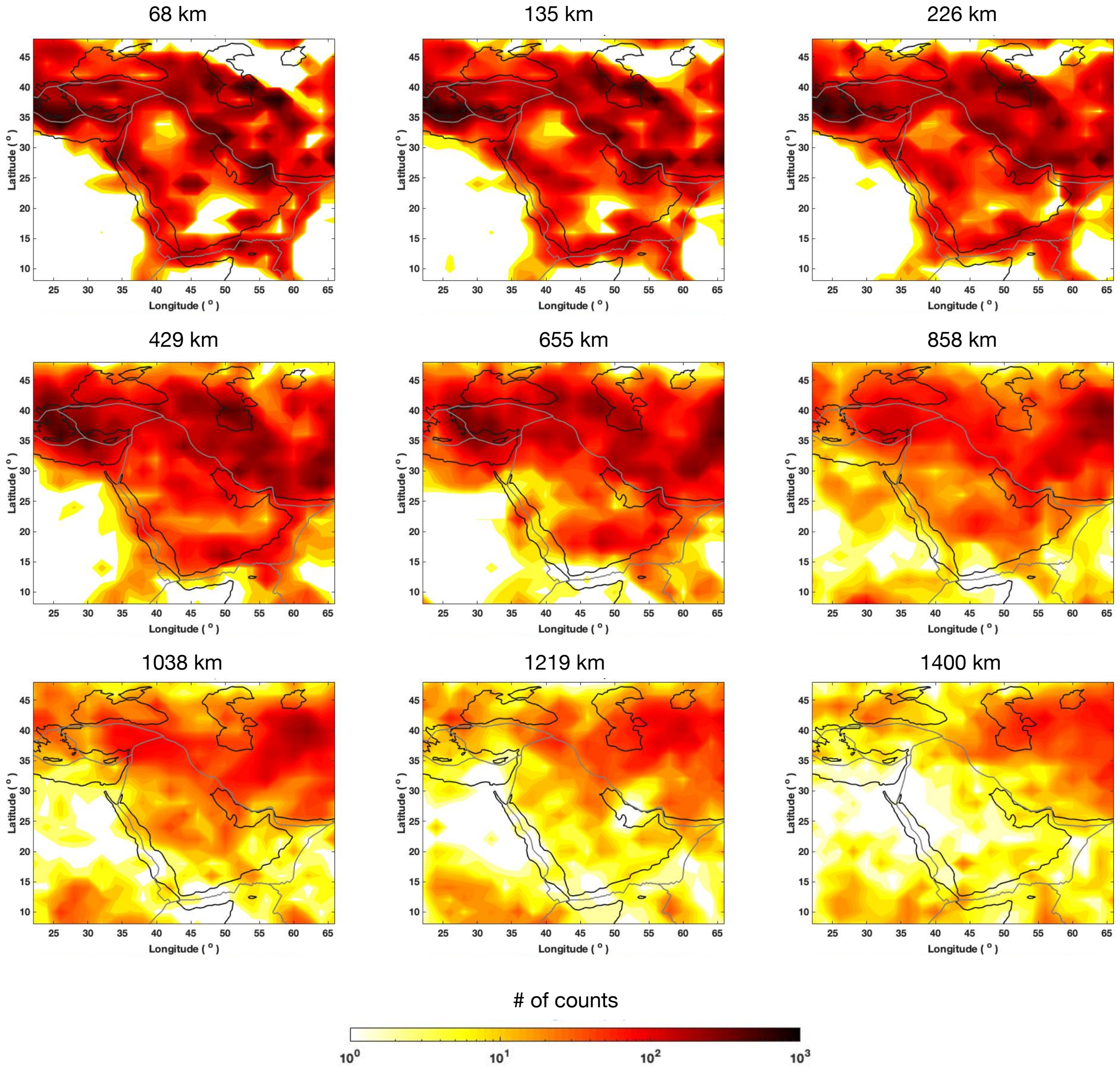

Figure 5 Density of hit counts of ray paths used in the inversion, in[cluding] the Arabian Peninsula, in 2°×2° cells, shown at various depths.

provement in data coverage is observed in the litho-sphere down to ~350–400 km underneath the Middle East.

In this study, we use the travel time inversion soft-ware package BD-Solve (Nolet, 2008) based on ray the-ory to invert for the compressional P-wave speed per-turbations with respect to the 1D reference model AK135 (Kennett et al., 1995). Since we use onset-time readings, ray theory should be valid where the first-order scattering effects can be neglected. To the first order, perturbations are defined as $\delta V_p = \Delta V_p/V_p^0$, where V_p and V_p^0 are the P wavespeeds in 3D and 1D models, respectively, and $\Delta V_p = V_p - V_p^0$. For the inverse problem we aim to obtain model parameters $m_i = (\frac{\Delta V_p}{V_p^0})_i$ defined on a cubed-Earth grid (Charlety et al., 2013) which has ~70 km size volume pixels (vox-els) on the surface with a total of ~3.6 million voxels cov-ering the globe from surface to the core-mantle bound-ary (CMB). The observed P-wave delay times, i.e. the difference between observed and predicted P-wave ar-rival times by the 1D reference model AK135, are

d_i, are the elements of d. The data v[...] the travel time sensitivity matrix A, computed by a 1D ray tracing algorithm. Th[e] Crust2.0 (Bassin, 2000) is used to corre[ct for] crustal perturbations by superi[mposing ...] which is used as the background m[odel ...] versions. In addition, the elli[pticity correction is ap]-plied to the data (Tian et al., 2007; Nolet, 2008).

We perform a ray-based lineariz[ed inversion to con]-struct a P-wave model of the stud[y region by solving the] linear equations

$$\mathbf{Am} = \mathbf{d}, \tag{1}$$

where m denotes the $M \times 1$ model vector, A is the $N \times M$ Jacobian matrix containing the partial derivatives of the data with respect to the model parameters. We [use a] damped least-squares inversion where mod[...]

timated such that

$$\mathbf{m} = (\mathbf{A}^{\mathbf{T}}\mathbf{C}_{\mathbf{d}}^{-1}\mathbf{A} + \gamma\mathbf{I})^{-1}\mathbf{A}^{\mathbf{T}}\mathbf{C}_{\mathbf{d}}^{-1}\mathbf{d}, \qquad (2)$$

where $\mathbf{C}_{\mathbf{d}}$ is the diagonal data covariance matrix, γ is the damping factor and $\mathbf{I}$ is the unit matrix. We then solve the following system of linear equations (Nolet et al., 2019)

$$\begin{pmatrix} \mathbf{A} \\ \epsilon_n \mathbf{I} \\ \epsilon_s \mathbf{D} \end{pmatrix} S^r \mathbf{y} = \begin{pmatrix} \mathbf{d} \\ 0 \\ 0 \end{pmatrix}, \qquad (3)$$

followed by

$$\mathbf{m} = S\mathbf{y}, \qquad (4)$$

where $\mathbf{D}$ has second order differences between model parameters, and ϵ_n and ϵ_s are the weights for norm damping and smoothing, respectively. As in Nolet et al. (2019), we also use one or two relaxation steps (represented by S^r) as preconditioners to smooth the solution towards one that satisfies $\nabla^2 m = 0$ where we fix the ratio ϵ_n/ϵ_s. Figs. S5-S10 show the χ^2 dependence on the number of relaxation steps (r) and damping parameter, parameterized by $\epsilon_n = (\mathrm{epsfac}) \times 30/(1-\mathrm{epsfac})$. We vary epsfac in a range of 0.0-1.0 to control the damping level from no-damping to high damping.

We derive error estimates for our arrival-time residuals using the method of Voronin et al. (2014) and its variant described by Nolet (2019). For the onset-time readings from the waveform data, we perform a manual selection excluding noisy data and traveltime residuals compared to AK135 that do not f[illegible] deviations as explained in Nolet and Lee (2022).

3 Results

To better understand the value of the arrival-time data from waveforms, we performed two sets of iterations: 1) with ISC data only and 2) with ISC data combined with the onset-time readings from waveforms recorded by the SGS network deployed on the Arabian Peninsula. Here, we present our results obtained by the combination of the ISC data with those from waveforms in the inversion, selected based on our checkerboard and L-curve tests. The readers are referred to the Supplementary Material for additional information including the inversion results with the ISC data only, vertical sections of the checkerboard tests for the ISC data with the arrival-time readings from waveforms and the L-curve tests.

In Figs. 6 and 7, we present the checkerboard test results of $4° \times 4°$ and $2.4° \times 2.4°$ cubed-checkers, respectively, with 4% P-wave speed perturbations, using the complete dataset (i.e., ISC data and the readings from waveforms) to understand the limitations of our data coverage. The $4° \times 4°$ checkerboard test results show that overall, we have good resolution down to $1{,}400$ km, which is better than ~ 400 km below [illegible] to ~ 1200 km covering a region including [illegible] part of the Red Sea. Although the [illegible] around $1{,}200$ km, we observe good resolution [illegible] tolia, the Arabian Peninsula, [illegible] $2.4° \times 2.4°$ [illegible]

resolution checkerboard test re… olution down to ~ 400 km and down to ~ 800 km where smear… ing occurs toward ~ 800 km. With the … lithosphere, the resolution is p… gap in resolution north of the Gul… additional arrival-time readin… nificantly improve the resolutio… the Arabian Peninsula (see Figs. … board results with the ISC data o… tions $2.4° \times 2.4°$ checkerboard tests (… are consistent with observation… tions and show good resolution down to ~ 600 km … ever we have good data coverage, … the south of the Arabian Peninsu… Red Sea. The additional data from … does not make much observable di… below ~ 429 km. We do not see signif… ment in our model below the litho… sphere since our ISC coverage is alrea… upper mantle because of the glob… P-wave arrival-time readings of … earthquake-receiver pairs wher… distance is $\sim 17°$ with corresponding turn… ~ 410 km depth in model AK135 (see F… data count histogram as a functi… tance). The checkerboard tests s… model has the best resolution in … can image $2.4° \times 2.4°$ structure in the Arab… sula as well as Anatolia and Iran … 60 km. Because of the global ISC da… its surrounding regions, the res… ~ 800 km especially for the large-s… lower mantle.

The norm damping and smoothing … plied in the inversion are chosen … tests shown in Figs. S7-S12. We ch… reduced chi-square of 0.8 for a value o… ing the standard data errors esti… data set, including the P-wave on… waveforms. The selection of inv… made with consideration based o… the checkerboard tests with pertu… shown in Figs. 6 & 7. Although the $2.4° \times 2.4°$ checker-board tests show reasonably good … ers $r=1$ with 1% damping, considering … ing and amplitude recovery, we s… higher damping 2% (see Fig. S10) …

Compared with the ISC data alone [illegible] $\sim$ in the … $1{,}000$ km, we show the horizontal sec… ious depths from 68 km down to 858 km inverted b… the combined data set of the ISC … readings from waveforms (Fig. 8). In addition [illegible] from wavefo… [illegible] within … [illegible], comp… [illegible] with the ISC da… [illegible]. We observe the shar… the Arabian shield and the Arabi… 300 km, taking advantage of the a… from waveforms, which is not that … [illegible] with the ISC data onl… [illegible] ~ 135 km, a low-velocity ano…

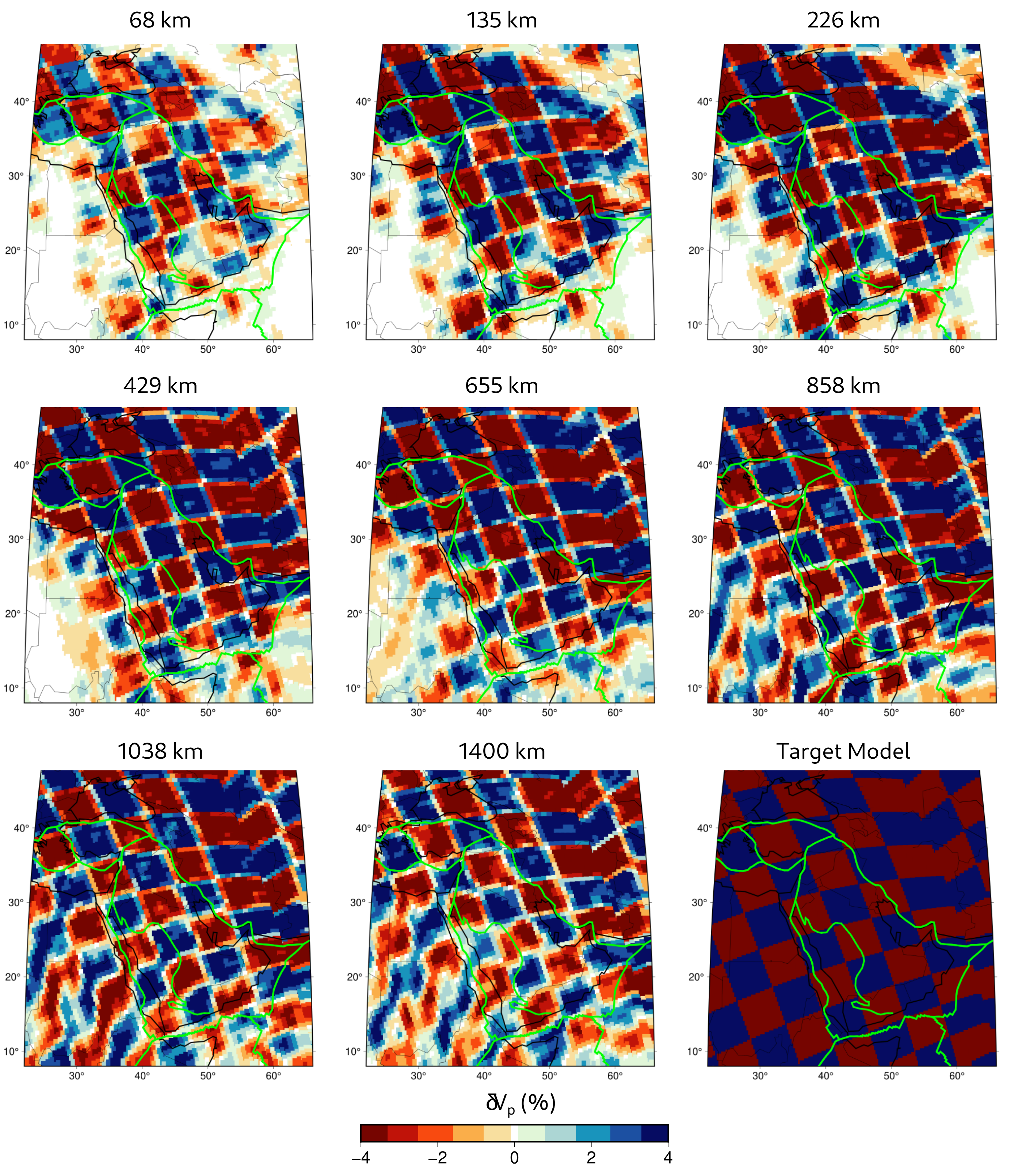

Figure 6 Horizontal cross-sections of the 4°×4° checkerboard test results for P-wave spe[...]
with the ISC data and onset-time readings from waveform data rec[...]

ing from Afar extends northward to the Caucasus, Egypt
which is well correlated with volcanism along the Red
Sea, in the Arabian shield and Eastern Anatolia. The
low-velocity anomaly along the Red Sea is shifted to the
East toward Harrats around 70 km, which is observed
just below the Red Sea around 200-km depth (Fig. 8),
consistent with previous models of the region (e.g., Kim
et al., 2023). The resolution on the western part of the

Red Sea (i.e., ~500 km) improve[...]
the global ISC data coverage.

We clearly observe the subducti[...]
arc (Fig. 9, sections AA′ - CC′) with po[...]
ments in the upper and lower mant[...]
responding checkerboard tests s[...]
power of data along the subducti[...]
turbations of the shallower Cyp[...]

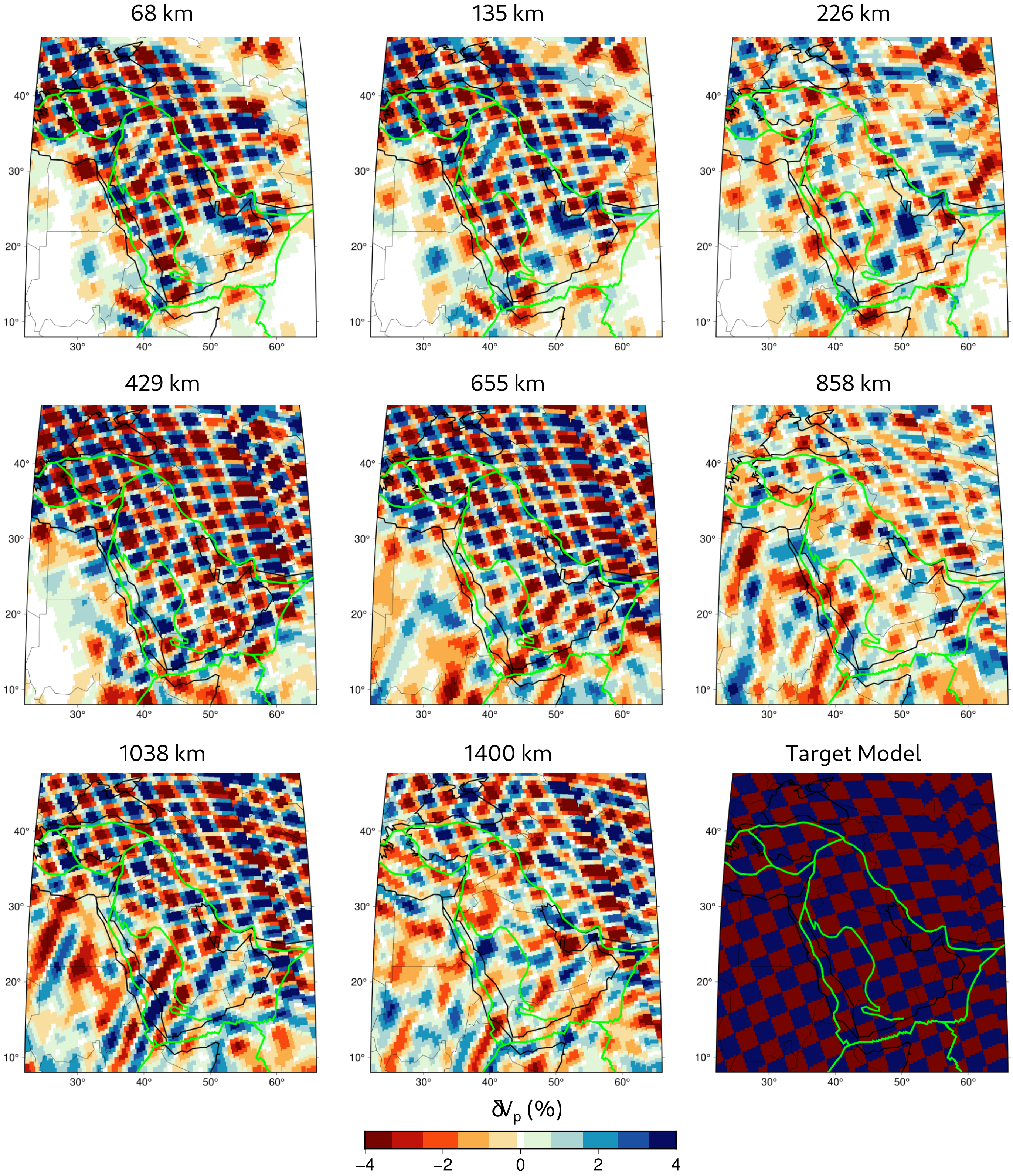

Figure 7 Same as Fig. 6 but for 2.4° × 2.4° checkerboard test results.

those of the Hellenic arc (Fig. 9, section CC'). The two low- … 200 km … 660 km … discontinuity undern… depth along sections DD' and EE' (Fig. 9, section FF') … The checkerboa… with the volcanic province Harrat … the same depth range sh… Syria and the volcanism in Eastern Anatolia (Fig. S5) the Caucasus, respectively. The low velocities in the litho- sphere underneath the Eastern and Central Anatolia are also clearly visible in section FF'. On the other hand, the potential remnant of the subduction along the Bitlis su-

The cross sections across the … show evidence of the eastern edge … lithosphere being underthruste… edge of the Eurasian plate (10; … et co…

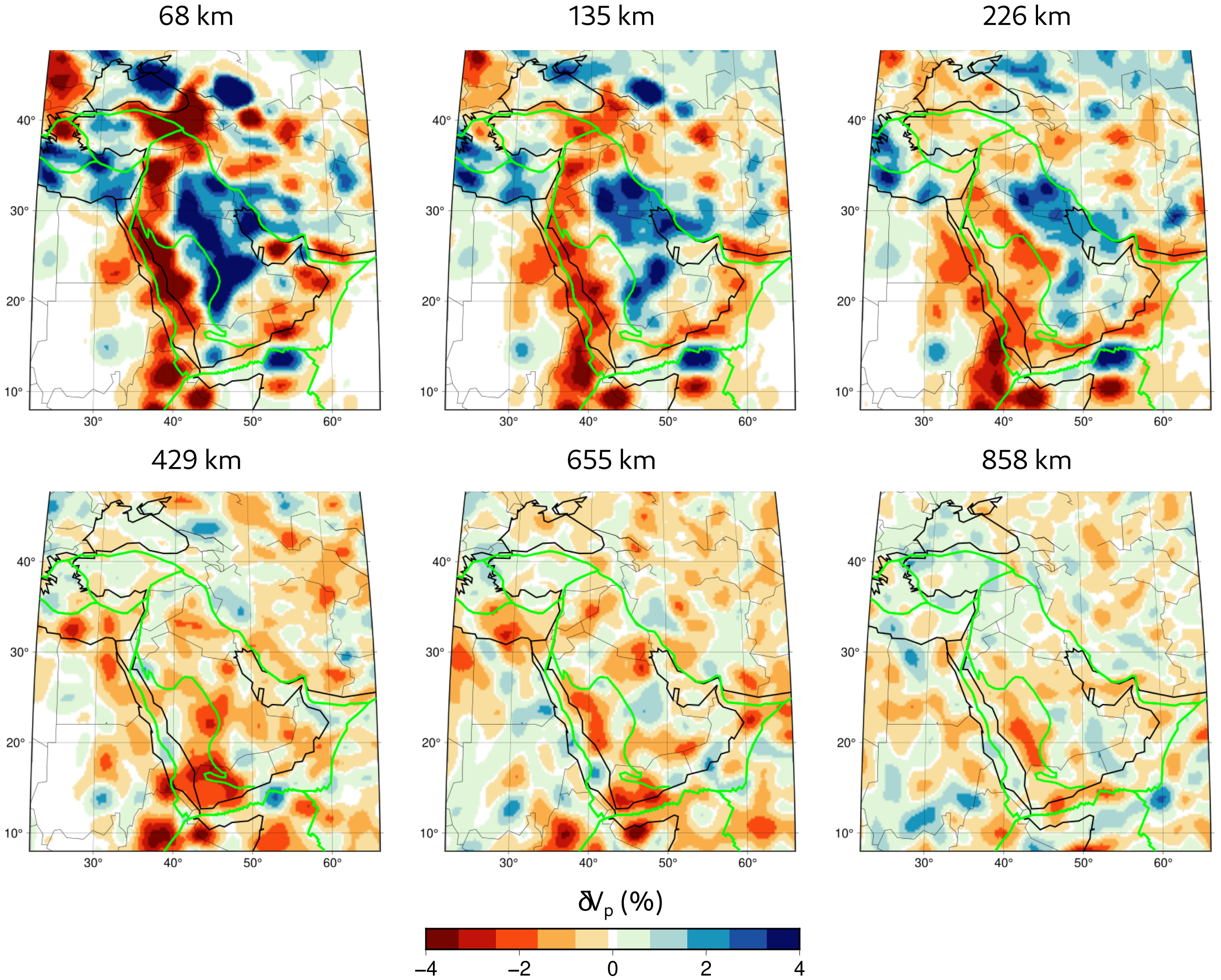

Figure 8 Horizontal cross-sections of P-wavespeed perturbations ... depths. ISC data combined with onset-time readings from wavef... version.

tions AA'-DD'). From sections AA'-DD', the subducted Tethys Ocean underneath Iran along the suture zone is visible down to 300 km. The subduction can be observed down to 660 km and penetrates the lower mantle with a steeper angle as we go towards the South. The checkerboard tests, in general, show good recovery along the Zagros suture zone and the East Caucasus, where ... to about 600 km depth, supporting the ... However, the resolution decreases towards the South in all sections in the Arabian plate, which is ... DD' (Fig. S6). The western part of the sections from AA' to DD' highlights the Red Sea and volcanism under the Harrats and Yemen, with low-velocity perturbations in the upper mantle extending to the lower mantle where the decreased checkerboard resolutions are observed correlated to the data coverage. The cross-sections along the Red Sea and the Arabian shield from South to North (EE'-FF') depict the channeled low-velocities with ... 300 km, which compare deeper in the South and extend to the lower mantle. Section GG' shows similar low-velocities on the southern edge while high-wavespeed perturbations characterize the litho-

... the Arabian platform to ... along the suture zone ... 300 km. The l... low-velocity zone in the southe... is well-correlated with the volc... going towards the Afar ... volcanism d... Zagros ... as well as the v... An anomaly ... East Caucasus ... Although the checkerboard ... for all secti... Red Sea are shown in sections CC' an... features are retrievable ...

In Fig. 11 we compare our model to th... Simmons (2021) the S-wave pe... Chang and Van der Lee (2011) and the P-wave perturbations of Celli (2020) in the uppe... mantle with respect to their mea... for perturbations with respect ... Simmons (2021) and Celli (2020) also have th... S-wavespeed models, which can b... Our P-wave perturbations are lar... global model Simmons (2021) where the l... velocity regions are better reso...

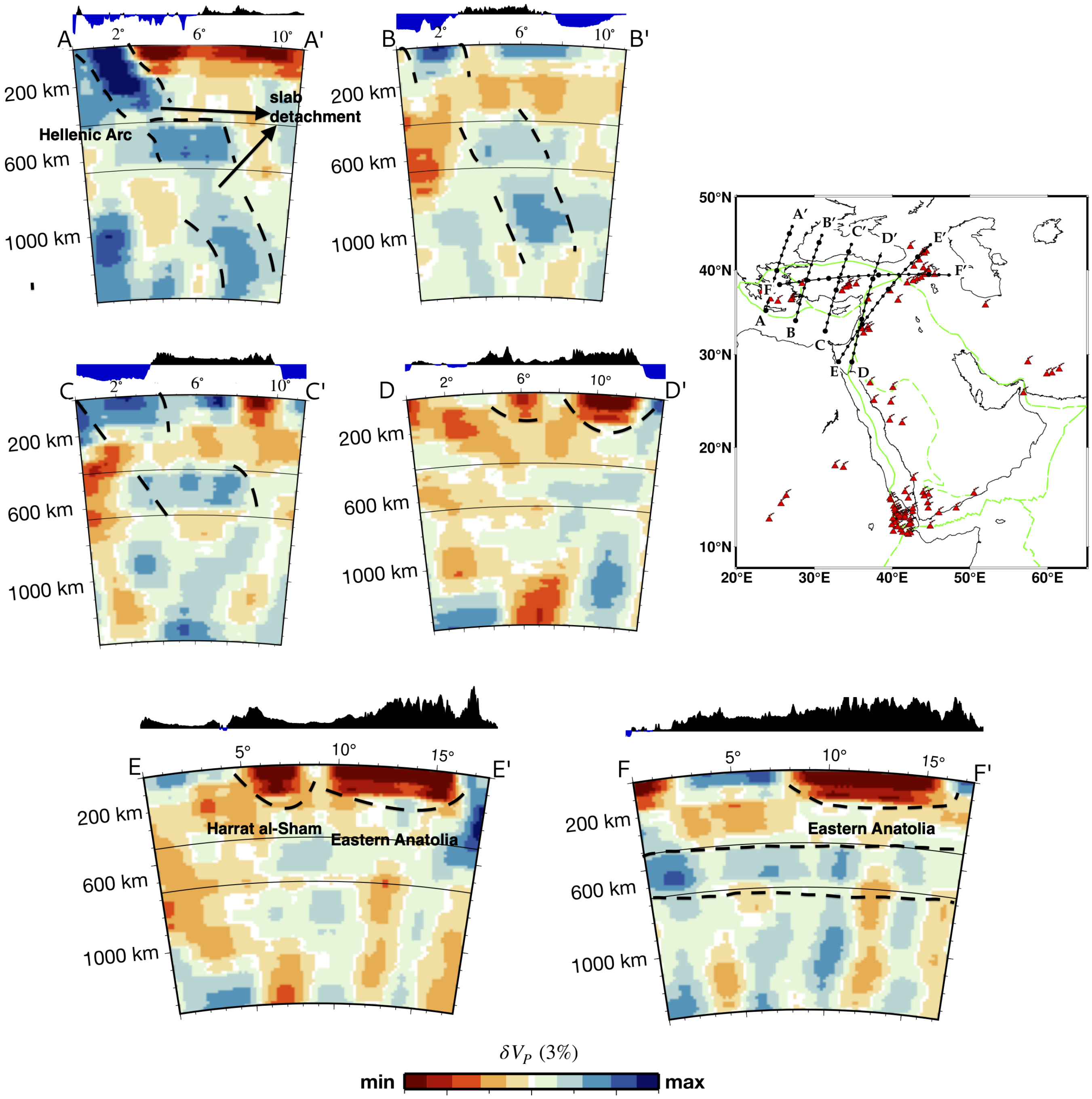

Figure 9 Same as Fig. 8 but for vertical sections traversing the Hellenic a

about 150 km. P- and S-wave speed models (Gelsi et al. ... where we can still clearly track
(2020) show the long-wavelength structure of ... Arabian ... studied platform d
region as a result of their construction (see Fig. S16) ... part of the northwest-s
African continent tomography. Overall, ... observed ... wave model b
length structures of the P and S wave models are consistent ... Chang and ... w
There is, in general, a good ... Van der Lee (2011) ... model around 450-
wave model Chang and Van der Lee (2011) S-wave ... also compare our model to the ver
model, where the main discrepancies ... Chang and Van der Lee (2011) along the re
Peninsula might be coming from ... different ... Fig. 12 ... largest discrepa
models and the additional data ... After ... section AA', wher
versions. We observe the largest discrepancy ... (Fig. S17) ... The (
200 km. The strong northwest-southeast ... low-wave speed anomali
velocity trend in the Arabian Peninsula ... BB' S-wave ... agree w
model Chang and Van der Lee (2011) and ... we have a decent resolution (Fig
ing P-wave model from Chang et al. ... speed anomaly in the Arabian
2012) around 200 km is less pronounced ... our model ... two potential man

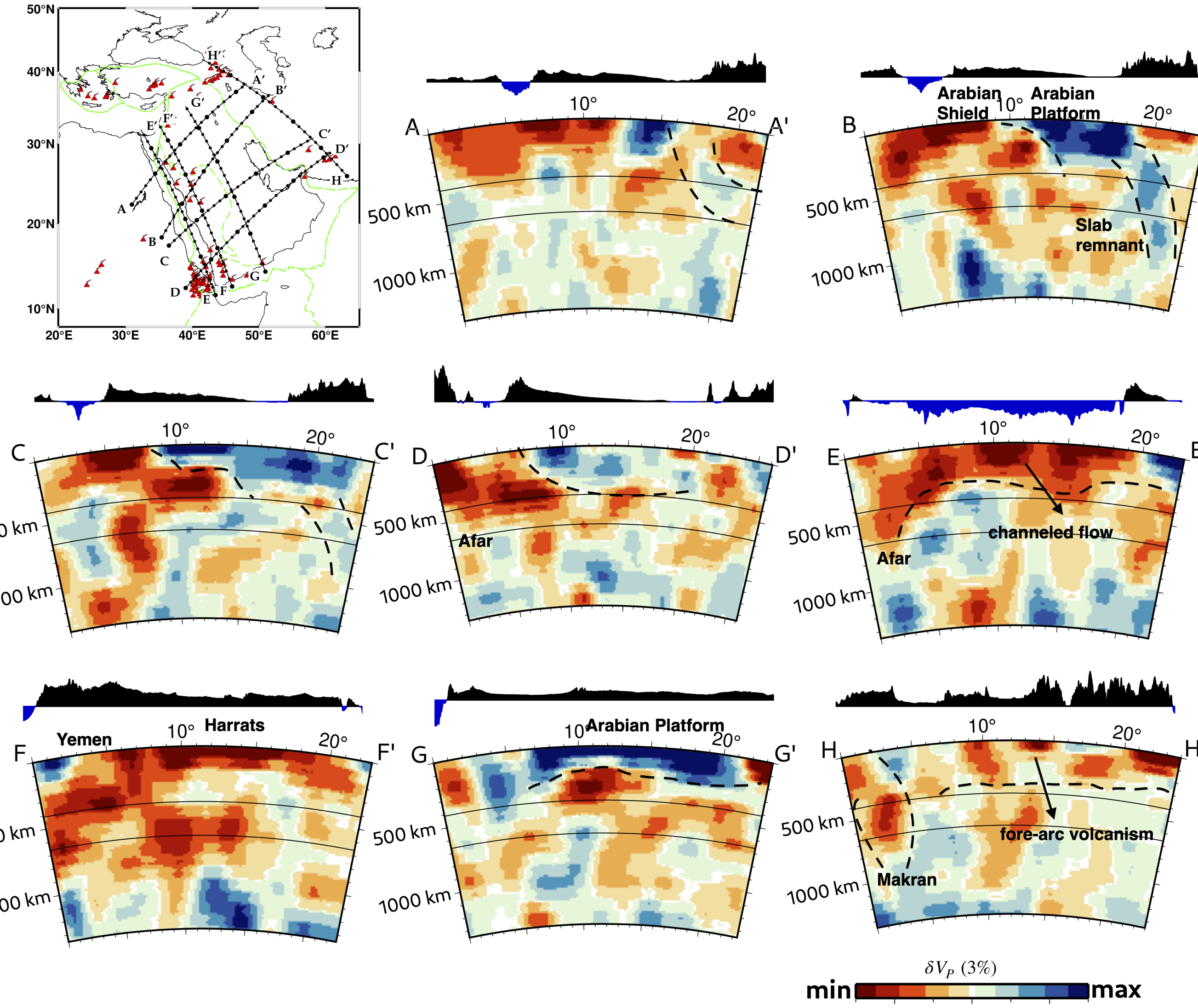

Figure 10 Same as Fig. 9 but for vertical sections traversing the Arabian s… suture zone.

by Chang and Van der Lee (2011) along the same … are also present in our model … in the lower mantle. Both models … tion along Zagros (section CC') … wavespeed anomalies surrounding … tend to the lower mantle. However, … extension of the subduction …

… reconstructed based on … Kim et al. (2012) and Carlile et al. (2020) … two tracks … part of t… African plate … upper … also show thi… together with 70 km … In our model, the … these two … likely exist … is more … identified, … 100 km from … to 200 km where we have good data coverage with th… time picks (Figs. 3 & 5). Kaviani et al. (2020) also observes this boundary around 90 km … the ambient-noise study in the same … lower resolution. Although it is …

4 Discussions

Our P-wave model, MEPT, shows the distinct separation of the Arabian platform and the Arabian shield, characterized by high- and low-wavespeed perturbations, respectively, in the upper mantle down to about 300 km (Fig. 8). The Arabian platform and the shield expose themselves clearly in the surface geology (Fig. 1). The boundary between these two tectonic units has also been reported in previous studies. For instance, Chang and Van der Lee (2011) observed … 75 km … based on their S-wave speed model of the region where the sharp discontinuity … Lim et al. (2020) also presents S-wave model based on the arrival times of S and SKS phases plotted starting at 100 km depth. The P and S-wave mod-

… directly, which is an upper mant… resolution in the crust, based o… the region, the wavespeed pertur… versed from the crust to the mant… platform is characterized by low… tions in the crust due to the sed… Mesopotamian Basin), and the Ara… acterized by relatively … (Bashir … et al., 2020; Kaviani, 2020a). The clear separ… tween the Arabian platform and th… and the upper mantle with the vel… consistent with a recent study o…

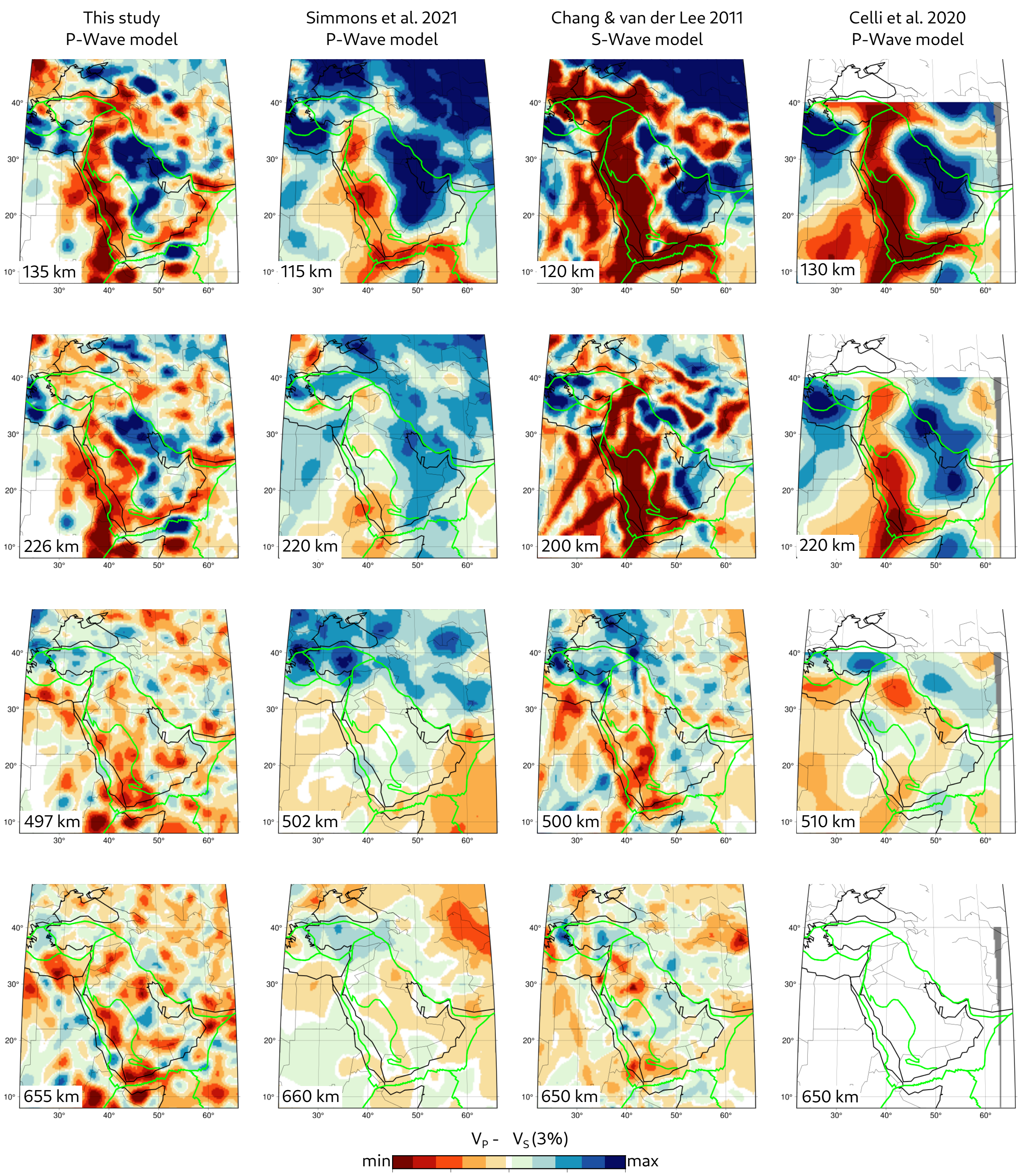

Figure C11 Comparison of the horizontal sections of the Simmons et al. (2021) P-wave and S-wave speed models of Chang and Van der Lee (2011), and the P-wave model of Celli et al. (2020) to the P-wave speed model of this study. Perturbations are plotted with respect to the mean ... S-wave speed cross-sections plotted with respect to AK135.

tle attenuation structure of the ... The region has slow Lg-wave speed ...
observations and measurements ... where the lithosphere ... Kaviani et al. ...
and upper mantle underneath the ... et al., 2020) is also supported by the Q model ...
form are characterized by low Q (high attenuation) ... Pasyanos et al. (2021) where the absence of L...
tor, the inverse of attenuation ~180 ... observed. On the other hand, the ...
and up ~ 5,600, respectively ... Pasyanos et al. (2021) in the platform compared to those ...

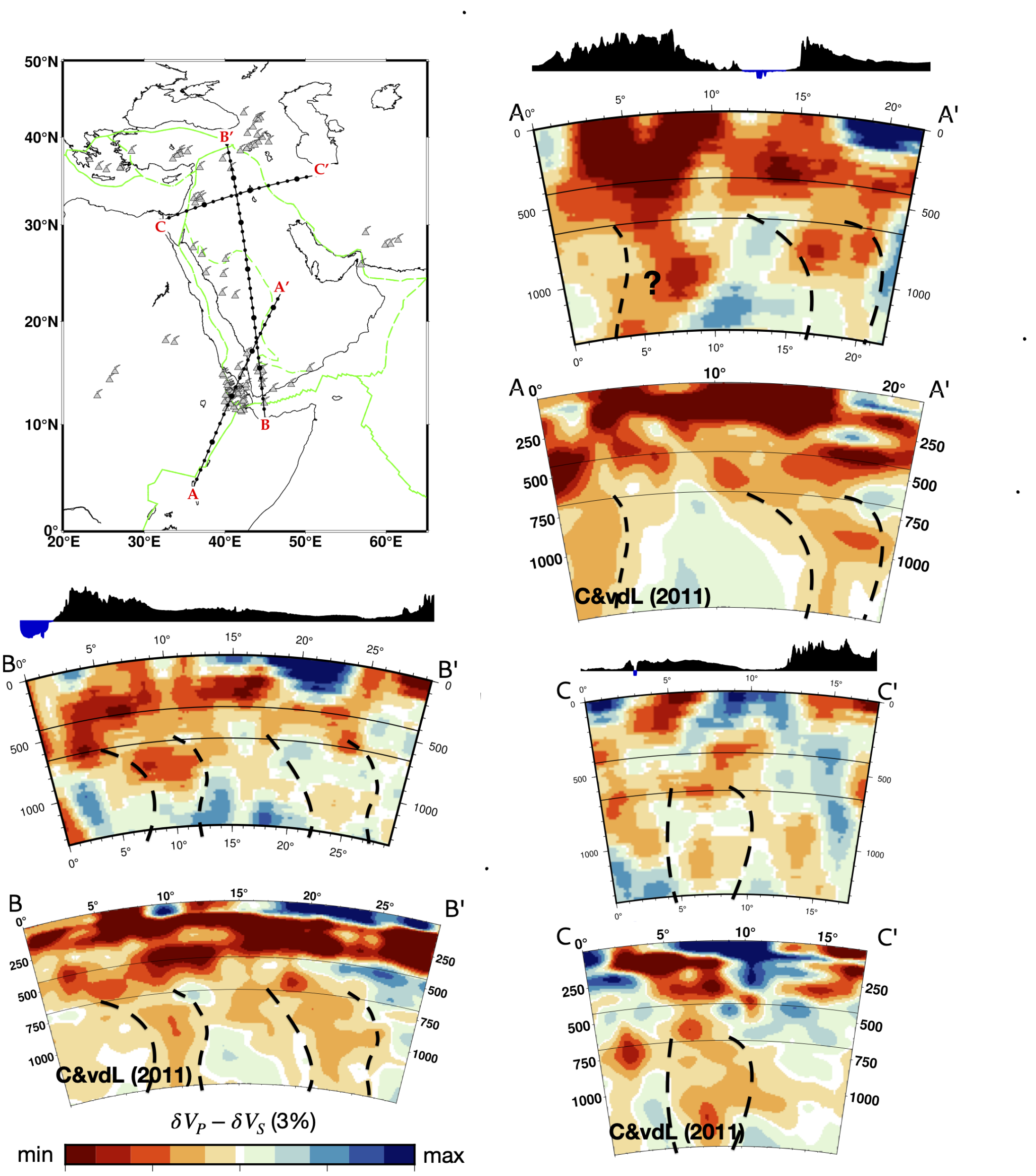

Figure 12 Comparison of the vertical sections of the S-wave model of Chang and Van der Lee (2011) and the P-wavespeed model from this study. Perturbations are plotted wit

serve in the upper mantle might [illegible] of the remnant of subduction along the Zagros collision zone. The slower P wavespeeds in the Arabian shield are likely related to the volcanism and the proposed plume models in the Arabian plate and spreading processes along the Red Sea (e.g., Koulakov et al., 2016; Pasyanos and Nyblade, 2007; Chang and Van der Lee, 2011).

There is no consensus on the origin of the volcanism of the Harrats, the largest continental alkali basalt province in Saudi Arabia extending from Yemen in the South to Syria, where there are records of historical eruptions close to major cities such as Medinah (e.g., Moufti and Németh, 2016). The low velocities observed along the Red Sea and Gulf of Aden are consistent with the continental rifting and spreading ridge. On the other hand, there is evidence for a channel of flow

northward to Eastern Anatolia or plume from geochemical data and s models (Ebinger and Sleep, 1998; Chang et al., 2011; Park et al., 2007) which is also suppor SKS observations in the rift region (Park et al., 2008) (Hansen et al., 2008). Our tomographic mode rule out the theory of spreading the region. However, the cross-s Sea (see Fig. 10) suggest the potential c from Afar to Syria with deeper and closer to Afar in the South. A sim also reported by Lim et al. (2020). Some global m els show the potential connectio the African superplume (e.g., Montelli et al., 2004; Ritsema et al., 2011; Lei et al., 2020) while some othe les propose regional plumes or ma neath the Arabian plate which ma

lated to Afar or the African superplume (Zhu et al., 2012). Similar anomalies along
scale (e.g., Chang et al., 2011; Koulakov, 2016). A
recent study by Kim et al. (2023) discusses that
model does not support a local plume
Arabian plate and cannot resolve
ported by Chang and Van der Lee (2011) and Koulakov et al. (2016). Our P-wave model seems
ing the mantle upwellings under
form and Jordan, supporting the
Chang and Van der Lee (2011) (Fig. 12; also see vertical
lution in Fig. S17). In addition,
of the channeled low-velocity
Peninsula observed in Chang and Van der Lee (2011) at
200 km (Fig. 11) is observed in our model
much deeper depth (350 km; Figs. 11 & S14), which
is likely another support for the local plumes by our
model.

Although the data coverage in the
lenic arc is not sufficient, the
arc are well resolved (Figs. 5, 7)
erage in Anatolia. The fast P-wave
related to the Hellenic arc (Fig. 9)
serve a potential slab
sections BB' and CC' in Fig. 9
board tests in Fig. S5). Similar
made in previous regional tomography
duced by surface waves (e.g.,
wave arrival times (e.g., Spakman et al., 1988;
2019) as well as the adjoint tomography
Zhu et al., 2012). We also observe a
ing in the lower mantle. The Hellenic slab
stagnant above 660 km before penetrating
mantle and appears at 1,000 km depth
stagnation was also reported by
2011; Piromallo and Morelli, 2003; Portner et al., 2018;
Wortel and Spakman, 2000), is likely the remnant of the
subducted and detached Tethys Ocean
tracked on an East-West section (Fig. 9)
As we move further East, at the
Cyprus arc, we observe a dipping
appears at 200–300 km, a possible tear
slab filled with hot material
on top of 660 km (Fig. 9). The fast anomaly
on top of the 660 km discontinuity
the subduction of the Tethys Ocean
lia (e.g., Biryol et al., 2011; Abgarmi et al., 2017). The
Aegean basin and Eastern Anatolia
by slow wavespeeds correlated with
related volcanism. The attenuation
previously attributed to the absence
mantle below in Eastern and central
Iranian Plateau (Gök et al., 2003). The pronounced
slow P wavespeeds we observe under
tolia and along the Zagros fold
high attenuation in these regions
absence of Sn waves and can indicate
sociated with the subduction and

We clearly observe fast-wavespeed perturbations
along the Bitlis suture zone in the upper mantle where
the remnant of the Tethys Ocean lies over the 660 km
discontinuity underneath Eastern Anatolia which was
also shown by the model of Biryol et al. (2011).

ture zone (Fig. 10) are also observed in the
studies underneath the Simav
plume (e.g., Salah and Zhao, 2003; Piromallo and
Ritzwoller, 2006; Chang and Van der Lee, 2011; Koulakov et al., 2016;
Koulakov and van der Lee, 2018) is associated with
The collision models of the
crease the potential of the Arabian plate double su
the observation history of the Neo-
(Jia et al., 2023). Although the observed
mantle extension of Z
Arabian the potential
further investigation is needed.

Seismic source studies require
and upper-mantle models of both P
P-wave speed models are more cha
structed mainly because of the re
S-wave speed mo
surface
tomographic model
sampling
the Arabian Peninsula
improvement in the resolution
underneath the Middle East
resolutions were caused b
information in this study is r
mantle depths because we used reg
our arrival-time tomography. Th
improved by u
events. In addition
(Bassin et al., 2000) during the inversion. We exp
crustal model (Laske et al.
successor of Crust2.0, s
overall conclusions. However, t
is well known, not only
(e.g., Bozdağ and Trampert, 2008; Ferreira et al., 2010)
(e.g., Ritsema et al., 2021), which may
have an impact on the inference pa
To minimize
the upper mantle, Moho perturb
as model parameters (Lee
and Nolet, 1997; Wiedtek et al., 2013). The simultan
crustal and upp
is the subject
within a full-waveform inversio
the resolution of th
collectively controlled by th
Cui et al. (2024) recently
balancing P
appropriate weigh
joint tomography framework. Com
another way
Our goal is
or mode
Such an appr
expand the study
sampled with emerging acoustic
MERMAIDs (Sukhovich et al., 2015) where the ons
time readings from MERMAID data ar
assimilated in a joint inversio
We also note that the recovery

checkerboard tests is not perfect, which is a common problem for traveltime tomographic studies for several reasons, such as data coverage, damping used in the inverse problem, etc. To further improve the resolution of the tomographic models of the region, full-waveform inversion (Tromp, 2019; Tape et al., 2009; Fichtner et al., 2017; Zhu et al., 2012) is the way forward, potentially with also carefully assimilating amplitudes of waveforms in inversions. However, although the inclusion of the amplitude information is desirable to constrain the heterogeneities better (e.g., Laske and Masters, 1996) as they are sensitive to the gradient of phase speeds (Woodhouse and Wong, 1986), the trade-off between wavespeeds, attenuation, and source uncertainties makes the inversions more challenging (e.g., Espindola-Carmona et al., 2024).

5 Conclusions

We present a higher-resolution P-wavespeed model, MEPT, of the Middle East and the surrounding region constructed based on teleseismic and regional arrival times of the first-arrival P waves collected from the most recently reinterpreted ISC-EHB bulletin (Engdahl et al., 2020) and onset-time readings from waveforms recorded by the Saudi Geological Survey (SGS) network on the Arabian Peninsula. The main strength of our model is the additional onset time readings from regional waveforms, which significantly improves the lithospheric and upper mantle structure specifically underneath the Arabian Peninsula.

Our model shows evidence of channeled flow northward from the Afar plume and supports the model of smaller mantle upwellings underneath the Arabian plate and Jordan to explain the origin of the volcanic fields in the region. The combined arrival times sharpen the boundary between the Arabian shield and the Arabian platform in the upper mantle, clearly observed down to 300-km depth. We also observe clear evidence of subducting the Hellenic and Cyprus arcs with potential slab tears, as well as the imprint of the collision along the Bitlis-Zagros suture zone following the closure of the Tethys Ocean. The observed slow P-wave anomalies in Eastern Anatolia and along the Zagros fold are likely related to the absence of the lithospheric mantle, which was previously interpreted by the attenuation of Sn waves.

In future studies, our goal is to assimilate the waveforms from the SGS network in an adjoint tomography setup to further improve the resolution through the simultaneous inversion of the crust and upper mantle for geological and tectonic interpretations as well as providing 3D reference models for source location and characterization studies. Ultimately, a framework that combines all available data (i.e., including arrival times in full-waveform inversion workflows) would be beneficial to improve the resolution of P-wavespeed models, which could potentially be extended to oceanic domains as well.

Acknowledgements

The authors thank Editor Suzan v… and reviewers for their constructive… reviews, which improved the manuscript. This study was s… Force Research Laboratory proje… FA9453-19-C-0068 and the Nation… with grant numbers EAR-1945565… The authors gratefully acknowl… data from the International Seis… EHB bulletin (http://www.isc.ac.uk/…) and wave… data from the Saudi Geologic…

Data and code availability

The traveltime inversion software … from https://www.geoazur.fr/GLOBAL… The P-wave model, MEPT, construc… available from Zenodo (https://doi.org/10.5281/zenod…). The P-wave arrival time data is … the International Seismologica… (http://www.isc.ac.uk). The wavefo… data used in this study is not op… maintained and provided by the S…vey.

Competing interests

Authors have no competing intere…

References

Abgarmi, B., Delph, J. R., Ozacar, A…, Sandvol, E., Türkelli, N., and Bi… crust and Arabian slab beneath the … from receiver functions: New insig… Geosphere, 13(6):1774–1787, … 10.1130/GES01509.1.

Adams, A., Brazier, R., Nyblade, A., … Source parameters for moderate … Zagros Mountains with implications f… … Bull. Seismol. Soc. Am., 99(3):2044–2049, … 10.1785/0120080314.

Agard, P., Omrani, J., Jolivet, L., a… history across Zagros (Iran): con… earlier … International Journal of … 94(3):401–419, 2005. doi: 10.1007/s00531-005-04…

Al-Damegh, K., Sandvol, E., Al-Lazk… seismic wave propagation (Lg and Sn… Arabian Plate … Geophys. J. Int., 157(2):775–795, 2004. doi: 10.1111/j.1365-246X.200…

Al-Lazki, A., Sandvol, E., Buland, S… N., and Mohamad, R. Pn tomographic i… locity and anisotropy at the junct… and African … Geophys. J. Int., 158(3):1024–1040, 2… doi: 10.1111/j.1365-246X.2004.02355…

Almalki, K. A., Betts, P. G., and Ail… geological and geophysical … Earth-Sci. Rev., 147:109–140, 2015. doi: 10.1016/j.earscirev.201…

Artemieva, I., Yang, H., and Thybo, H. Incipient ocean spreading beneath the Arabian Shield. Earth-Sci Rev, 226:103955, 2022. doi: 10.1016/j.earscirev.2022.103955.

Augustin, N., van der Zwan, F., Devey, C., and Brandsdóttir, B. 13 million years of seafloor spreading throughout the Red Sea Basin. Nat Commun, 12:2427, 2021. doi: 10.1038/s41467-021-22586-2.

Ball, P., Roberts, G., Mark, D., Bafadhil, W. W., [illegible] Nahdi, M., and Garni, S. Geochemical and geochronological analysis of Harrat Rahat, Saudi Arabia [illegible] lated intraplate [illegible]. Lithos, 446-447:107112, 2023. doi: 10.1016/j.lithos.2023.107112.

Bassin, C., Laske, G., and Masters, G. The current limits of resolution for surface wave tomography in North America. EOS, 81:F897, 2000.

Bijwaard, H., Spakman, W., and Engdahl, E. R. Closing the gap between regional and global travel time tomography. Journal of Geophysical Research: Solid Earth, 103(B12):30055–30078, 1998. doi: 10.1029/98JB02467.

Bird, P. An updated digital model of plate boundaries. Geochemistry, Geophysics, Geosystems, 4(3):1027, 2003. doi: 10.1029/2001GC000252.

Biryol, C., Beck, S. L., Zandt, G., and Özacar, A. Segmented African lithosphere beneath the Anatolian region inferred from teleseismic P-wave tomography. Geophys J Int, 184:1037–1057, 2011. doi: 10.1111/j.1365-246X.2010.04910.x.

Bonatti, E. Punctiform initiation of seafloor spreading in the Red Sea during transition from a continental to an oceanic rift. Nature, 316:33–37, 1985. doi: 10.1038/316033a0.

Bozdağ, E. and Trampert, J. On Crustal Corrections in Surface Wave Tomography. Geophysical Journal International, 172(3):1066–1082, Mar. 2008. doi: 10.1111/j.1365-246X.2007.03690.x.

Bozdağ, E., Peter, D., Lefebvre, M., Komatitsch, D., Tromp, J., Hill, J., Podhorszki, N., and Pugmire, D. Global adjoint tomography: first-generation model. Geophys J Int, 207(3):1739–1766, 2016. doi: 10.1093/gji/ggw356.

Bozkurt, E. Neotectonics of Turkey – a synthesis. Geodin Acta, 14(1-3):3–30, 2001. doi: 10.1080/09853111.2001.11432432.

Braunmiller, J. and Nábělek, J. Geometry of continental normal faults: seismological constraints. Journal of Geophysical Research, 101(B2):3045–3052, 1996. doi: 10.1029/95JB02882.

Braunmiller, J., Kradolfer, U., Baer, M., and Giardini, D. Regional moment tensor determination in the European-Mediterranean area—initial results. Tectonophysics, 356(1-3):5–22, 2002. doi: 10.1016/S0040-1951(02)00374-8.

Camp, V. and Roobol, M. Upwelling asthenosphere beneath Western Arabia and its regional implications. J Geophys Res, 97:15255–15271, 1992. doi: 10.1029/92JB00943.

Camp, V. E., Hooper, P. R., Roobol, M. J., and White, D. The Madinah eruption, Saudi Arabia: magma mixing and simultaneous extrusion of three basaltic chemical types. Bull Volcanol, 49(2):489–508, 1987. doi: 10.1007/BF01245475.

Celli, N., Lebedev, S., Schaeffer, A., and Gaina, C. African cratonic lithosphere carved by mantle plumes. Nat Commun, 11:92, 2020. doi: 10.1038/s41467-019-13871-2.

Chang, S.-J. and Van der Lee, S. Mantle plumes and associated flow beneath Arabia and East Africa. Earth Planet Sci Lett, 302(3):448–454, 2011. doi: 10.1016/j.epsl.2010.12.050.

Chang, S.-J., Van der Lee, S., and Flanagan, M. P. A new P-velocity model for the Tethyan margin from a scaled S-velocity model and the inversion of P- and PKP-delay times. Physics of the Earth and Planetary Interiors, 211-212:1–7, 2012. doi: [illegible]

Charléty, J., Voronin, S., Nolet, G., [illegible] K., and Daubechies, I. C. Global seismic tomography with sparsity constraints: Comparison with smoothing and damping regularization. Journal of Geophysical Research: Solid Earth, 118(9):4887–4899, 2013. doi: 10.1002/jgrb.50326.

Chiang, A., Gök, R., Tarabulsi, Y. M., [illegible] Bafadhil, W. W., [illegible] Seismic [illegible]. Arabian Journal of Geosciences, 14(2): [illegible], 2021. doi: 10.1007/s12517-020-0 [illegible]

Civilini, F., Mooney, W. D., Savage, M. K., [illegible] The crust [illegible] Harrat [illegible] Geophys J Int, 219(3):1532– [illegible], 2019. doi: 10.1093/gji/ggz380.

Coleman, R. G., [illegible] Journal of [illegible] 77–100, [illegible] doi: 10.1016/0040-1951(88)90296-X.

Cui, C., Lei, W., Liu, Q., Peter, D., Bozdağ, E., Tromp, J., Hill, J., Podhorszki, N., and Pugmire, D. GLAD-M35: a joint P and S global tomographic model with uncertainty quantification. Geophys J Int, 239(1):478–502, 2024. doi: 10.1093/gji/ggae270.

Debayle, E., [illegible] inversion [illegible] sets: Model construction and [illegible] J Geophys Res, [illegible] 2004. doi: 10.1029/2003jb00265 [illegible]

Delaunay, A., Baby, G., [illegible] Structural and morphological evolution of the Eastern Red Sea [illegible] morphology, uplift processes and [illegible] Earth-Science Reviews, 250:104698, 2024. doi: https://doi.org/10.1016/j.earscirev.202 [illegible]

Duncan, R. A., Kent, A. J., Thornber, [illegible] Amri, A. M. Timing and composition of [illegible] Harrat Hutaymah, western Saudi Arabia [illegible] Journal of Volcanology and Geothermal Research, 313:1–14, 2016. doi: https://doi.org/10.1016/j.jvolgeores.20 [illegible]

Ebinger, C. and Sleep, N. Cenozoic magmatism throughout East Africa resulting from impact of a single plume. Nature, 395:788–791, 1998. doi: https://doi.org/10.1038 [illegible]

Engdahl, E., Di Giacomo, D., Sakarya, [illegible] J., and Storchak, D. ISC-EHB 1964-20 [illegible] studies of Earth structure [illegible] Earth and Space Sci, 7:e2019EA000897, 2020. doi: 10.1029/2019EA000 [illegible]

Engdahl, E. R., Jackson, J. A., Myers, [illegible] Priestley, K. Relocation and assessment [illegible] Iran region. Geophysical Journal International, 167(2):761– [illegible], 2006. doi: 10.1111/j.1365-246x.2006.03 [illegible]

Espindola-Carmona, A., Örsvuran, [illegible] ter, D. B. [illegible] Geophysical Journal International [illegible] Science, 236(2):952–966, 2024. doi: [illegible]

Ferreira, A. M. G., Woodhouse, J. H., [illegible] the Robustness of Global Radially A [illegible] mography. Journal of Geophysical Research, 115(B4), 2010. doi: 10.1029/2009JB006716.

Fichtner, A., Kennett, B. L. N., Ige [illegible] waveform tomography for radially a [illegible] insights into present and past stat [illegible] mantle. Earth and Planetary Science Letters, 290:270–280, 2010. doi: 10.1016/j.epsl.2009.12.003.

Giardini, D., Basham, P., and Berry, [illegible] hazard assessment program [illegible] Natural [illegible] as step to protecting vulnerable com [illegible] Conference held in London, pages [illegible]

Thomas Telford Publishing, 1993.

Giardini, D., Danciu, L., Erdik, M., Şeşetyan, K., Tümsa, M. B. D., Akkar, S., Gülen, L., and Zare, M. Seismic hazard map of the Middle East. Bulletin of earthquake engineering, 16(8): 3567–3570, 2018. doi: 10.1007/s10518-018-0347-3.

Gök, R., Kaviani, A., Matzel, E. M., Pasyanos, M. E., Mayeda, K., Yetirmishli, G., El-Hussain, I., Al-Amri, A., Al-Jeri, F., Godoladze, T., et al. Moment magnitudes of local/regional events from 1D coda calibrations in the broader Middle East region. Bull. Seismol. Soc. Am., 106(5): 1926–1938, 2016. doi: 10.1785/0120160045.

Gök, R., Sandvol, E., Türkelli, N., Seber, D., and Barazangi, M. Sn attenuation in the Anatolian and Iranian plateau and surrounding regions. Geophys. Res. Lett., 30(24): 8042, 2003. doi: 10.1029/2003GL018020.

Gök, R., Pasyanos, M. E., and Zor, E. Lithospheric structure of the continent-continent collision zone: eastern Turkey. Geophys. J. Int., 169(3): 1079–1088, 2007. doi: 10.1111/j.1365-246x.2006.03288.x.

Hansen, S. E., Rodgers, A. J., Schwartz, S. Y., and Al-Amri, A. M. Imaging ruptured lithosphere beneath the Red Sea and Arabian Peninsula. Earth and Planetary Science Letters, 259(3-4): 256–265, 2007. doi: 10.1016/j.epsl.2007.04.035.

Hansen, S. E., Gaherty, J. B., Schwartz, S. Y., Rodgers, A. J., and Al-Amri, A. M. Seismic velocity structure and upper-mantle anisotropy in the Red Sea and Arabian peninsula from surface wave analysis. Journal of Geophysical Research: Solid Earth, 113(B10), 2008. doi: 10.1029/2007jb005335.

Hatzfeld, D. and Molnar, P. Comparisons of the kinematics and deep structures of the Zagros and Himalaya and of the Iranian and Tibetan plateaus and geodynamic implications. Reviews of Geophysics, 48(2), 2010. doi: 10.1029/2009rg000304.

International Seismological Centre

Jafari, A., Ao, S., Jamei, S., and Ghasemi, H. Evolution of the Zagros sector of Neo-Tethys: Tectonic and magmatic events that shaped its rifting, seafloor spreading and subduction history. Earth-Sci. Rev., 241: 104419, 2023. doi: 10.1016/j.earscirev.2023.104419.

Karasözen, E., Nissen, E., Bergman, E. A., Johnson, K. L., and Walters, R. J. Normal faulting in the Simav graben of western Turkey reassessed with calibrated earthquake relocations. Journal of Geophysical Research: Solid Earth, 121(6): 4553–4574, 2016. doi: 10.1002/2016jb012828.

Karasözen, E., Nissen, E., Bergman, E. A., and Ghods, A. Seismotectonics of the Zagros (Iran) from orogen-wide, calibrated earthquake relocations. Journal of Geophysical Research: Solid Earth, 124(8): 9109–9129, 2019. doi: 10.1029/2019jb017336.

Kaviani, A., Paul, A., Bourova, E., Hatzfeld, D., Pedersen, H., and Mokhtari, M. A strong seismic velocity contrast in the shallow mantle across the Zagros collision zone (Iran). Geophysical Journal International, 171(1): 399–410, 2007. doi: 10.1111/j.1365-246x.2007.03535.x.

Kaviani, A., Paul, A., Moradi, A., Mai, P. M., Pilia, S., Boschi, L., Rümpker, G., Lu, Y., Tang, Z., and Sandvol, E. Crustal and uppermost mantle shear wave velocity structure beneath the Middle East from surface wave tomography. Geophysical Journal International, 221(2): 1349–1365, 2020. doi: 10.1093/gji/ggaa075.

Kennett, B. L., Engdahl, E., and Buland, R. Constraints on seismic velocities in the Earth from traveltimes. Geophysical Journal International, 122(1): 108–124, 1995. doi: 10.1111/j.1365-246x.1995.tb03540.x.

Khrepy, S. E., Koulakov, I., Gerya, T., Al-Arifi, N., Alajmi, M., and Qadrouh, A. Transition from continental rifting to ocanic spreading in the northern Red Sea. Sci. Rep., 11: 5594, 2021. doi: 10.1038/s41598-021-84952-w.

Kin, R., Witek, M., Chang, S.-J., Lin tropic and radially anisotropic beneath the Arabian plate inferred from raphy. Tectonophysics, 862: 229968, 2023. https://doi.org/10.1016/j.tecto.2023.22

Kiuchi, R., Mooney, W. D., and Zahran, H. Earthquakes from the Saudi Ar Bull. Seismol. Soc. Am., 109(5): 1722–1737, 2019. doi: 10.1785/0120180302.

Koulakov, I., Burov, E., Cloetingh, S., El Khrepy, S., Al-Arifi, N., and Bushenkova, N. Evidence for anomal mantle beneath the Arabian Platform from tr Tectonophysics, 667: 176–188, 2016. https://doi.org/10.1016/j.tecto.2015.11

Laske, G. and Masters, G. Constraints on global phase velocity maps from long-period polarization data. J. Geophys. Research: Solid Earth, 101(B7): 16059–16075, 1996. doi: 10.1029/96jb00526.

Laske, G., Masters, G., Ma, Z., and Pasyanos, M. Update on CRUST1.0 - A 1-degree Global Model of Earth's Crust. In EGU General Assembly, Geophys. Res. Abstracts, 15: EGU2013-2658, 2013.

Le Pichon, X. and Kreemer, C. The Miocene-to-present kinematic evolution of the Eastern Mediterranean and Middle East and its implications for dynamics. Annual Review of Earth and Planetary Sciences, 38: 323–351, 2010. doi: 10.1146/annurev-earth-040809-152419.

Lebedev, S. and van der Hilst, R. D. Global upper-mantle tomography with the automated multimode inversion of surface and S-wave forms. Geophys. J. Int., 173(2): 505–518, 2008. doi: 10.1111/j.1365-246x.2008.03721.x.

Lei, W., Ruan, Y., Bozdağ, E., Peter, D., Lefebvre, M., Komatitsch, D., Tromp, J., Hill, J., Podhorszki, N., and Pugmire, D. Global Adjoint Tomography—Model GLAD-M25. Geophys. J. Int., 223(1): 1–21, 2020. doi: 10.1093/gji/ggaa253.

Li, X.-D. and Romanowicz, B. Global mantle shear velocity model developed using nonlinear asymptotic coupling theory. J. Geophys. Res., 101(B10): 22245–22272, 1996. doi: 10.1029/96JB01306.

Liu, K., Lee, C., Chang, S., Mai, P. M., and flow of plume material ben S wave traveltime tomography. J. Geophys. Research: Solid Earth, 125: e2020JB019668, 2020. https://doi.org/10.1029/2020JB019668.

Maggi, A. and Priestley, K. Surface waveform tomography of the Turkish–Iranian plateau. Geophysical Journal International, 160(3): 1068–1080, 2005. doi: 10.1111/j.1365-246x.2005.02505.x.

McClusky, S., Balassanian, S., Barka, A., Demir, C., Ergintav, S., Georgiev, I., Gurkan, O., Hamburger, M., et al. Global Positioning System constraints on plate kinematics and dynamics in the eastern Mediterranean and Caucasus. Journal of Geophysical Research, 105(B3): 5695–5719, 2000. doi: 10.1029/1999jb900351.

McKenzie, D. The structure of the lithosphere beneath the Eastern Mediterranean and Middle East. Mediterranean Geoscience Reviews, 2: 311–326, 2020. https://doi.org/10.1007/s42990-020-0003

Meier, T., Becker, D., Endrun, B., Rische, M., Bohnhoff, M., Stöckhert, B., and Harjes, H. A model for the Hellenic subduction zone in the area of Crete based on seismological investigations. Geological Society, London, Special Publications, 291(1): 183–199, 2007. doi: 10.1144/sp291.9.

Mokhtar, T. A. and Al-Saeed, M. M. Shear wave velocity structures of the Arabian Peninsula. Tectonophysics, 230(1-2):105–125, 1994. doi: 10.1016/0040-1951(94)90149-x.

Montelli, R., Nolet, G., Masters, G., Dahlen, F., and Hung, S.-H. Global P and PP traveltime tomography: rays versus waves. Geophys. J. Int., 158(2):637–654, 2004. doi: 10.1111/j.1365-246X.2004.02346.x.

Moufi, M. R. and Németh, K. The Geoheritage Value of the Youngest Long-Lived Volcanic Field in the Kingdom of Saudi Arabia, pages 33–120. Springer International Publishing, Cham, 2016. doi: 10.1007/978-3-319-33015-0_3.

Mukhopadhyay, B., Mogren, S., Mukhopadhyay, M., and Dasgupta, S. Incipient status of dyke intrusion in top crust–evidences from the Al-Ays 2009 earthquake swarm, Harrat Lunayyir, SW Saudi Arabia. Geomatics, Natural Hazards and Risk, 4(1):30–48, 2013. doi: 10.1080/19475705.2012.663794.

Nissen, E., Tatar, M., Jackson, J. A., and Allen, M. B. New views on earthquake faulting in the Zagros fold-and-thrust belt of Iran. Geophysical Journal International, 186(3):928–944, 2011. doi: 10.1111/j.1365-246x.2011.05119.x.

Nissen, E., Jackson, J., Jahani, S., and Tatar, M. Zagros "phantom earthquakes" reassessed—The interplay of seismicity and deep salt flow in the Simply Folded Belt? Journal of Geophysical Research: Solid Earth, 119(4):3561–3583, 2014. doi: 10.1002/2013jb010796.

Nolet, G. A breviary of seismic tomography. A Breviary of Seismic Tomography by Guust Nolet. Cambridge, UK: Cambridge University Press, 2008. doi: 10.1017/cbo9780511984709.

Nolet, G. and van der Lee, S. Error estimates for seismic body wave delay times in the PSD-ISC Bulletin. Geophys. J. Int., 231(3):1739–1749, 2022. doi: 10.1093/gji/ggac282.

Nolet, G., Hello, Y., Van der Lee, S., Bonnieux, S., Ruiz, M. C., Pazmino, N. A., Deschamps, A., Regnier, M. M., Font, Y., Chen, Y. J., and Simons, F. J. Imaging the Galápagos mantle plume with an unconventional application of floating seismometers. Scientific Reports, 9:1326, 2019. doi: 10.1038/s41598-018-36835-w.

Pallister, J. S., McCausland, W. A., Jónsson, S., Lu, Z., Zahran, H. M., El Hadidy, S., Aburukbah, A., Stewart, I. C., Lundgren, P. R., White, R. A., et al. Broad accommodation of rift-related extension recorded by dyke intrusion in Saudi Arabia. Nature Geoscience, 3(10):705–712, 2010. doi: 10.1038/ngeo966.

Parisi, L., Augustin, N., Trippanera, D., Kirk, H., Dannowski, A., Matrau, R., Fittipaldi, M., Nobile, A., Zielke, O., Valero Cano, E., Hoogewerf, G., Aspiotis, T., Manzo-Vega, S., Espindola Carmona, A., Barreto, A., Juchem, M., Suhendi, C., Schmidt-Aursch, M., Mai, P. M., and Jónsson, S. The First Network of Ocean Bottom Seismometers in the Red Sea to Investigate the Zabargad Fracture Zone. Seismica, 3(1):104698, 2024. doi: https://doi.org/10.26443/seismica.v3i1.729.

Park, Y., Nyblade, A., Rodgers, A., and Al-Amri, A. Upper mantle structure beneath the Arabian Peninsula and northern Red Sea from teleseismic body wave tomography: Implications for the origin of Cenozoic uplift and volcanism in the Arabian Shield. Geochem. Geophys. Geosyst., 8:Q06021, 2007. doi: 10.1029/2006GC001566.

Park, Y., Nyblade, A. A., Rodgers, A. J., and Al-Amri, A. S-wave velocity structure of the Arabian Shield upper mantle from Rayleigh wave tomography. Geochemistry, Geophysics, Geosystems, 9(7), 2008. doi: 10.1029/2007gc001895.

Pasyanos, M. E. and Walter, W. R. Crust and upper-mantle structure of North Africa, Europe and the Middle East from inversion of surface waves. Geophysical Journal International, 149(2):463–481, 2002. doi: 10.1046/j.1365-246X.2002.01663.x.

Pasyanos, M. E., Walter, W. R., and Ha … study of the Middle East and … the Comprehensive Nuclear-Test-Ban … Comprehensive Nuclear Test Ban Tr … pages 1445–1474. Springer, 2001. doi: 10.1007/978-3-0348 …

Pasyanos, M. E., Tarabulsi, Y. M., Al … Mousa, A. D., El-Hussain, I., Al-J … R. Improved lithospheric attenuat … Peninsula through the use of … Arabian Journal of Geosciences, 14(9):14, 2021. doi: 10.1007/s12517-021-0 …

Piromallo, C. and Morelli, A. P wave t … der the Alpine-Mediterranean area. Journal of Geophysical Research, 108:2065, 2003. doi: 10.1029/2002jb00175 …

Portner, D. E., Delph, J. R., Biryol, … Özacar, A. Subduction termination … formation across Eastern Mediterra … updated P-wave tomography. Geosphere, 14: 907–925, 2018. doi: 10.1130/ges01617.1.

Reilinger, R. and McClusky, S. Nubi … tions and the dynamics of Mediterra … tonics. Geophys. J. Int., 186(3):971–979, 2011. doi: 10.1111/j.1365-246X.2011.05133.x.

Reilinger, R., McClusky, S., Vernan … Cakmak, R., Ozener, H., Kadirov, F … et al. GPS constraints on continent … Arabia-Eurasia continental collis … the dynamics of plate interactions. Journal of Geophysical Research: Solid Earth, 111(B5), 2006. doi: 10.1029/2005jb0 …

Ring, U., Glodny, J., Thomas Will, T … lenic Subduction System: High-Pre … humation, Normal Faulting, and Lar … Rev. Earth Planet. Sci., 38:45–76, 2010. doi: 10.1146/an … nurev.earth.050708.170910.

Ritsema, J., Rivera, L. A., Komatits … ist, H.-J. Effects of crust and mantl … SS/S amplit … Geophysical Research Letters, 29(10):72–1, 2002. doi: 10.1029/2001GL013831.

Ritsema, J., Deuss, A., Van Heijst, H … a degree-40 shear-velocity model … Rayleigh wave dispersion, telesei … mode splitting function … Geophys. J. Int., 184(3):1223–1236, 2011. doi: 10.1111/j.1365-246x.20 …

Rodgers, A. J., Krischer, L., Afanas … and Simmons, N. Adjoint Waveform T … and Upper Mantle Structure of the M … Asia for Improved Waveform Simulat … able Broadband Data. Bull. Seismol. Soc. Am., 2024. doi: https://doi.org/10.1785/0120230248.

Royden, L. The tectonic expression … tal convergent boundaries. Tectonics, 12(2):3 …, 1993. doi: 10.1029/92tc02248.

Sandvol, E., Seber, D., Barazangi, M., Vernon, F., Mellors, R., and Al-Amri, A. Lithospheric seismic velo … the Arabian Shield. Geophys. Res. Lett., 25(15):2873–2876, 1998. doi: 10.1029/98gl02214.

Sanfilippo, A., Cai, M. Y., Jácome, R. A … and Al Amri, A. … Harrat Lunayyir and Khaybar Vo … pages 389–415. Springer International P … 10.1007/978-3-319-99408-6_18.

Schaeffer, A. J. and Lebedev, S. Global … tle and transition zone. Geophys. J. Int., 194(1):417–4 … doi: 10.1093/gji/ggt095.

Schettino, A., Macchiavelli, C., Pi …

sul, N. Recent kinematics of the tectonic plates surrounding the Red Sea and Gulf of Aden. Geophys. J. Int., 207(1):457–480, 2016. doi: 10.1093/gji/ggw280

Sen, P., Temel, A., and Gourgaud, A. Petrogenetic modelling of Quaternary post-collisional volcanism: a case study of central and eastern Anatolia. Geol. Mag., 141(1):81–98, 2004. doi: 10.1017/S0016756803008550

Şengör, A., Görür, N., and Şaroğlu, F. Strike-slip faulting and related basin formation in zones of tectonic escape: Turkey as a case study. Strike-Slip Deformation, Basin Formation, and Sedimentation, ed. Kevin T. Biddle and Nicholas Christie-Blick, Special Publications of SEPM, 1985. doi: https://doi.org/10.2110/pec.85.37.0211

Shapiro, N. M. and Ritzwoller, M. H. Monte-Carlo inversion for a global shear-velocity model of the crust and upper mantle. Geophysical Journal International, 151:88–105, 2002. doi: 10.1046/j.1365-246x.2002.01742.x

Shedlock, K. M., Giardini, D., Grunthal, G., and Zhang, P. The GSHAP global seismic hazard map. Seismological Research Letters, 71(6):679–686, 2000. doi: 10.1785/gssrl.71.6.679

Simmons, N. A., Myers, S. C., Johannesson, G., and Matzel, E. LLNL-G3Dv3: Global P wave tomography model for improved regional and teleseismic travel time prediction. J. Geophys. Res.: Solid Earth, 117(B10), 2012. doi: 10.1029/2012jb009525

Simmons, N. A., Myers, S. C., Morency, C., Chiang, A., and Knapp, D. R. SPiRaL: A Multiresolution Global Tomography Model of Seismic Wave Speeds and Radial Anisotropy Variations in the Crust and Mantle. Geophysical Journal International, 227(2):1366–1391, Nov. 2021. doi: 10.1093/gji/ggab277

Sonder, L. J. and England, P. C. Effects of a temperature-dependent rheology on large-scale continental extension. Journal of Geophysical Research, 94(B6):7603–7619, 1989. doi: 10.1016/0148-9062(90)90013-r

Spakman, W., Wortel, M., and Vlaar, N. The Hellenic subduction zone: A tomographic image and its geodynamic implications. Geophysical Research Letters, 15(1):60–63, 1988. doi: 10.1029/gl015i001p00060

Sukhovich, A., Bonnieux, S., Hello, Y., Irisson, J.-O., Simons, F. J., and Nolet, G. Seismic monitoring in the oceans by autonomous floats. Nature Communications, 6(1):8027, 2015. doi: 10.1038/ncomms9027

Tang, Z., Julià, J., Zahran, H., and Mai, P. M. The lithospheric shear-wave velocity structure of Saudi Arabia: young volcanism in an old shield. Tectonophysics, 680:8–27, 2016. doi: 10.1016/j.tecto.2016.05.004

Tang, Z., Mai, P. M., Chang, S.-J., and Zahran, H. Evidence for crustal low shear-wave speed in western Saudi Arabia from multi-scale fundamental-mode Rayleigh-wave group-velocity tomography. Earth and Planetary Science Letters, 495:24–37, 2018. doi: 10.1016/j.epsl.2018.05.011

Tang, Z., Mai, P. M., Julià, J., and Zahran, H. Shear velocity structure beneath Saudi Arabia from the joint inversion of P and S wave receiver functions, and Rayleigh wave group velocity dispersion. Journal of Geophysical Research: Solid Earth, 124(5):4767–4787, 2019. doi: 10.1029/2018jb017131

Tape, C., Liu, Q., Maggi, A., and Tromp, J. Adjoint tomography of the southern California crust. Science, 325(5943):988–992, 2009. doi: 10.1126/science.1175298

Tarantola, A. Inversion of seismic reflection data in the acoustic approximation. Geophysics, 49(8):1259–1266, 1984. doi: 10.1190/1.1441754

Tavakoli, B. and Ghafory-Ashtiany, M. Seismic hazard assessment of Iran. Annali di Geofisica, 42(6):1013–1021, 1999. doi: 10.4401/ag-3781

Tian, Y., Hung, S.-H., Nolet, G., Mon
namic ray tracing and traveltime co
tomography. Journal of Computational Physics, 226(1):672–
2007. doi: 10.1016/j.jcp.2007.04.025

Tkalčić, H., Pasyanos, M. E., Rodge
and Al-Amri, A. A multistep approac
face wave dispersion and teleseism
cations for lithospheric structure
of the Arabian Peninsula. Journal of Geophysical Research, 111(B11), 2006. doi: 10.1029/2005JB004130

Trampert, J., Deschamps, F., Resovs
abilistic tomography maps chemica
Science, 306(5697):853–856
doi: 10.1126/science.1101996

van der Lee, S. and Nolet, G. Upper ma
North America. J. Geophys. Res., 102(B10):22815–2
doi: 10.1029/97JB01168

Viltres, R., Jónsson, S., Alothman,
F., Doubre, S., and Reilinger, R. P
Tectonics, 41(2):e2021TC007013, 2022. doi: https://doi.org/10.1029/2021TC

Voronin, S., Mikesell, D., Slezak, I
mographic linear systems: size red
Geophysical Journal International, 199(1):276–285,
doi: 10.1093/gji/ggu242

Wei, W., Zhao, D., Wei, F., Bai, X., a
the Eastern Mediterranean and Midd
P-Wave Anisotropic Tomography. Ge
Geosystems, 20:4505–4530, 2019. doi: 10.1029/2019GC0

Weinstein, Y., Navon, O., Altherr,
Lithospheric Mantle Heterogeneit
Pleistocene Alkali Basaltic Suite
(Israel). Journal of Petrology, 47(5):1017–1050,
doi: 10.1093/petrology/egl003

Witek, M., Lee, S.-M., Chang, S.-J.,
version of large datasets for radia
Geophys. J. Int., 232(2):1311–1339, 2023. doi: 10.1093/gji/g

Woodhouse, J. and Wong, Y. Amplitude
of mantle waves. Geophys. J. R. astr. Soc., 87:753–773, 19
10.1111/j.1365-246X.1986.tb0197

Wortel, M. and Spakman, W. Subductio
the Mediterranean-Carpathian region. Science, 290(5498):1910–19
2000. doi: 10.1126/science.290.5498.19

Zhu, H., Bozdağ, E., Peter, D., and T
ropean upper mantle revealed by adj
Nature Geoscience, 5(7):493–498, 2012. doi: 10.1038/ngeo1501